REVIEW

Check for updates

Formulation of PLGA nano-carriers: specialized modification for cancer therapeutic applications

Manosree Chatterjee [ID] *[ab] and Nripen Chanda [ID] *[a]

The eminence of nano-scale materials prevailed after the invention of high-resolution microscopes. Nowadays, nanoparticles are predominantly found in every application, including biomedical applications. In nanomedicine, the unique properties make nano-scale particles an efficient delivery vehicle to overcome the adverse effects of therapeutic molecules, which are directly administered. The polymeric nanoparticles have gradually gained interest as a nano-carrier over various non-polymeric types of nanoparticles due to their biocompatible nature. PLGA is the most frequently used polymer to synthesize polymeric nano-carriers as it is a clinically approved biodegradable polymer and has a broad scope of modification of its inherent properties. PLGA polymer, before or after nanoparticle formation, can be functionalized using various non-covalent and covalent modification techniques to suit desired applications. Since the beginning of PLGA nanoparticle usage, different synthesis methods have evolved progressively with various advantages and limitations. The present review also discusses the post-surface modification characterization of PLGA nanoparticles and their imaging and drug delivery applications.

1 Introduction

The concept of nanoparticles was theoretically introduced in the 19th century by Max Planck and Albert Einstein, which gradually became an imperative field after the invention of the transmission electron microscope.[1] From the beginning of the 20th century, nano-materials gained more attention after flourishing sophisticated high-resolution characterization techniques and became a promising technology for a wide range of applications.[1,2] In 1908, Paul Ehrlich, who won the Nobel Prize in Medicine, has given the concept of ''magic bullet'', which was a carrier of drug molecules with another agent of selectivity that only destroys diseased cells without any harmful effect on healthy cells.[1] Nowadays, nanoparticles'

[a] Material Processing and Microsystem Laboratory, CSIR – Central Mechanical Engineering Research Institute, Durgapur-713209, India. E-mail: manosree87@gmail.com, n_chanda@cmeri.res.in; Fax: +91-343-2546745; Tel: +91-9474112053, +91-9933034370

[b] Department of Biotechnology, National Institute of Technology Durgapur, Durgapur-713209, India

Dr Manosree Chatterjee has completed her PhD degree from the Department of Biotechnology, National Institute of Technology Durgapur (NIT Durgapur), India, in October 2021. She obtained her Master's degree in Biochemistry from The University of Burdwan, India. She has more than six years of research experience and published ten research articles. She has received CSIR-Senior Research Fellow award in Trans Disciplinary Research in 2018. In her doctoral research, she focused on the synthesis of biocompatible and monitorable nano-drug carrier systems with self-sensing drug release properties for cancer therapeutic applications.

Manosree Chatterjee

Dr Nripen Chanda currently serves as Principal Scientist in Materials Processing and Microsystems Laboratory, CSIR-CMERI, Durgapur. He obtained his PhD from the Indian Institute of Technology Bombay and worked for seven years as a Postdoctoral Research Associate at the University of Missouri-Colombia, USA. His current activities include designing and developing micro/nanoscale devices such as sensors, actuators, drug delivery systems, and processes for interdisciplinary research in biomedical/environmental engineering. He has published more than 75 research articles and 7 patents so far.

Nripen Chanda

unique physicochemical properties make them an indispensable aspect of biomedical research that has both monitoring and therapeutic applications in disease.[3–5] Its nano-scale size provides (i) high surface area to volume ratio that can accommodate a massive amount of external agents, (ii) distinctive optical property, which can help in imaging, (iii) electrical property with specific zeta (ζ) potential significant for interaction with cells, (iv) chemical property that can deliver an opportunity for functionalization with small molecules, and (v) colloidal stability, which helps in the application by preventing irreversible aggregation.[6–10] Different kinds of nanoparticles, such as polymeric, metallic, and liposome nanoparticles, were meticulously investigated to treat many lethal diseases, and many of them are in clinical trials.[11–15] Detection and monitoring of pathologies are essential to identify the disease and its intensity.[16] Iron oxide, gold, and gadolinium nanoparticle have proven their potentials in magnetic resonance imaging (MRI).[17,18] Various metallic nanoparticles are used in computerized tomography (CT), ultrasound, photoacoustic imaging, positron emission tomography, and optical imaging.[19–25] Though several drug delivery systems have been effectively used in clinical practices, a major constraint of such systems, specifically with metallic nanoparticles (e.g., silver nanoparticles) is bio-accumulation over the due course of treatment. Since the metal-based nanoparticles are not metabolized in physiological conditions, prolonged treatment with such nano-formulations leads to undesirable complications.[26,27]

These limitations can be addressed by polymer-based biocompatible nano-materials that have emerged as an alternative platform for drug delivery and imaging applications. Among all types of US Food and Drug Administration (FDA) approved nanoparticles used as a drug delivery system, polymeric nanoparticles are the most widely used in clinical practices.[15] In addition to the biocompatibility, the polymeric nanoparticles offer a few other advantages, e.g., (a) enhancing the encapsulation of small molecules, (b) preventing degradation or deactivation of the drug in the bloodstream before reaching the target, (c) prolonging blood circulation time, (d) controlling the release of drugs in target tissues or cells, (e) improving the drug loading capacity, (f) increasing the bioavailability of drugs, and finally (g) speeding the passive accumulation of drugs at tumor sites based on the enhanced permeability and retention (EPR) effect.[28–32] Besides, there is a flexibility to modify its pristine polymer chain and surface characteristics to enhance drug delivery and imaging efficacy, making them a superior therapeutic nano-platform.

The majority of the polymeric nanoparticles are fabricated using numerous biocompatible polymers to reduce the undesirable systemic toxicity of the drug transporter.[33] Among these, FDA and European Medicine Agency (EMA) approved biodegradable PLGA polymer is most widely used as a versatile and clinically proved elemental polymer for the synthesis of efficient nano-carriers.[34–36] Simultaneous drug enrichment to the tumor site and minimizing toxicity to normal tissues are indispensable aspects of nanoparticle-mediated drug delivery purposes. The use of biocompatible polymers like PLGA to achieve these aspects through nanoparticle synthesis has been

an ever-growing arena in the field of safe drug delivery. PLGA polymer is composed of varying ratios of lactic acid and glycolic acid monomer units that are ester bonded to form the polyester polymer. In an in vivo system, PLGA polymer decomposed upon hydrolysis at the ester bond and eventually metabolized through the kerbs cycle with the nontoxic end products (H_2O and CO_2), which are eliminated from the body.[37–39] The globally accepted and clinically approved PLGA polymer chains randomly orient themselves to form PLGA nanoparticles (Fig. 2). PLGA copolymers with low molecular weights ($M_W < 10$ kDa) are synthesized by the polycondensation reaction of lactic acid and glycolic acid in various ratios and higher molecular weight copolymers (generally used 10–100 kDa) are synthesized by ring-opening polymerization of cyclic dimers (Fig. 2).[35,39] Biodegradation of PLGA nanoparticles depends on the integral properties of the PLGA copolymer chain, which include the ratio of lactic acid and glycolic acid monomers in its chain composition and molecular weight.[36,40] The drug release from PLGA nanoparticles by the degradation of PLGA copolymer can be regulated by tuning the ratio of lactic acid and glycolic acid monomers in the PLGA chain. If the ratio of lactic acid is increased in the PLGA chain, the hydrophobicity also increases proportionally, resulting in a slow degradation of PLGA as it absorbs less water.[35,36,40] On the contrary, faster hydrolysis is observed when the glycolic acid content in PLGA is higher, resulting in the rapid release of drugs from nanoparticles. An acid-terminated PLGA chain with lower molecular weight and equal ratio of lactic acid (LA) and glycolic acid (GA) (50 : 50 PLGA) is frequently used to prepare drug delivery vehicles due to its optimum degradation rate (less than two months at 37 °C in an aqueous medium).[35,41,42] PLGA copolymer with higher molecular weight causing slower degradation rate of nanoparticles exhibits a slower drug release.[40] Various clinically significant biomolecules are efficiently encapsulated inside the PLGA nanoparticle's core through weak covalent interactions for imaging and drug delivery. The physicochemical properties of nanoparticles predominantly depend on the composition and molecular weight of the PLGA polymer.[39] The polymer can be dissolved in a wide range of organic solvents like acetone, dichloromethane, tetrahydrofuran, ethyl acetate, and chloroform, which is advantageous for nanoparticle synthesis.[38] Moreover, PLGA nanoparticles prove its excellence as a nano-carrier system as it possesses a wide range of degradation rates that provide a desirable formulation opportunity, stability in long-term storage, and high encapsulation efficiency. The first targeting (prostate-specific membrane antigen (PSMA)–targeted) nanomedicine BIND-014 containing docetaxel, which was tested on humans, was prepared with PLGA polymer.[43,44] Currently available PLGA polymer-based antitumor drugs approved for clinical practices to treat various types of cancer are listed in Table 1.[45–51]

In the present study, we review the synthesis, surface properties, and superiority of PLGA nano-carriers towards cancer therapeutic applications. It includes a comprehensive discussion on the existing PLGA nanoparticle synthesis methods, surface functionalization processes, and subsequent characterization techniques. It also covers the optimization and limitations of the existing PLGA nano-formulation procedures. Finally, we scrutinized the

Table 1   PLGA based anti-tumor drugs approved by FDA

Product (manufacturers' name)	Drug name	Dosage type	PLGA content and LA : GA	Drug dosages	Targeted tumor	Approved year
Decapeptyl® (Ferring Pharmaceuticals Pvt. Ltd.)	Triptorelin	Microsphere	50 : 50	3.75 mg in every 28 days for 6 months	Prostate, breast	1986
Zoladex Depot® (AstraZeneca UK Limited)	Goserelin acetate	Implant	13.3–14.3 mg per dose; 50 : 50	3.6 mg in every 28 days	Prostate	1989
Lupron Depot® (Abbvie Endocrine Inc)	Leuprolide	Microsphere	33.1 mg per dose; 75 : 25	3.75 mg in every month	Prostate	1989
Sandostatin Lar® (Novartis Pharmaceuticals UK Ltd)	Octreotide acetate	Microsphere	188.8,377.6 and 566.4 mg per dose; 50 : 50 (glucose-initiated PLGA)	10 mg, 20 mg or 30 mg in every 4 weeks	Acromegaly	1998
Trelstar® (Ferring Pharmaceuticals Pvt.)	Triptorelin pamoate	Microsphere	136, 118, 182 mg per dose; 78 : 22	3.75 mg in every 4 weeks or 11.25 mg in every 12 weeks or 22.5 mg in every 24 weeks	Prostate	2000
Eligard® (Zydus Cadila Healthcare Ltd.)	Leuprolide acetate	*In situ* forming implant	82.5 mg per dose of 50 : 50 (in 7.5 mg), 158.6 mg per dose of 75 : 25 (in 22.5 mg), 211.5 mg per dose of 75 : 25 (in 30 mg) and 165 mg per dose of 85 : 15 (in 45 mg)	1 mg in every day 7.5 mg in a month 22.5 mg in every 3 months 30 mg in every 4 months 45 mg in every 6 months	Prostate	2002
Signifor Lar® (Novartis Pharmaceuticals Corporation)	Pasireotide pamoate	Microsphere	26.29, 52.58, 78.87 mg per dose of PLGA-50-60 : 40–50 and PLGA-50 : 50	20 mg, 40 mg, 60 mg in every 28 days	Acromegaly	2014

theranostic efficiency of the PLGA nano-carrier system, a promising alternative to conventional drugs. Then, we have summarized the reported research on the cancer therapeutic applications of the PLGA nano-carrier. The review's complete structure is depicted in Fig. 1. This review article provides an extensive understanding of all the milestones for making a

PLGA nano-carrier, which is a potential cancer therapeutic system.

2 Synthesis techniques of PLGA nanoparticles

Synthesis techniques of PLGA nanoparticles depend on their application and the type of molecules they have to encapsulate. Therefore, it is required to select an appropriate synthesis method for the proper designing of nanoparticles. The size distribution and shape of PLGA nanoparticles are mainly determined by the PLGA chain orientation and parameters of the synthesis method. The synthesis method also has a strong influence on the colloidal stability, encapsulation efficiency of the external agents, and behavior of the nanoparticles in the cellular model. Moreover, the release rate of the encapsulated agent depends on the synthesis parameters of the particular synthesis procedure.[39] Here, the existing synthesis procedures are discussed in two categories. First, the comparatively older methods are denoted as conventional methods, and second, the comparatively newer ones are denoted as non-conventional methods. The process parameters, critical characteristics of the synthesized particles, advantages, and limitations of the methods are tabulated in Table 2.

2.1   Conventional methods

The most frequently applied earlier methods for the synthesis of PLGA nanoparticles in this category are discussed below.

2.1.1   Emulsion-solvent evaporation method. Emulsion solvent evaporation is the most frequently used technique to encapsulate small drug molecules, macromolecules (protein, DNA), and magnetic nanoparticles inside PLGA nanoparticles.[52–55] In this method, hydrophobic and hydrophilic molecules are encapsulated by physical adsorption through the formation of an oil–water
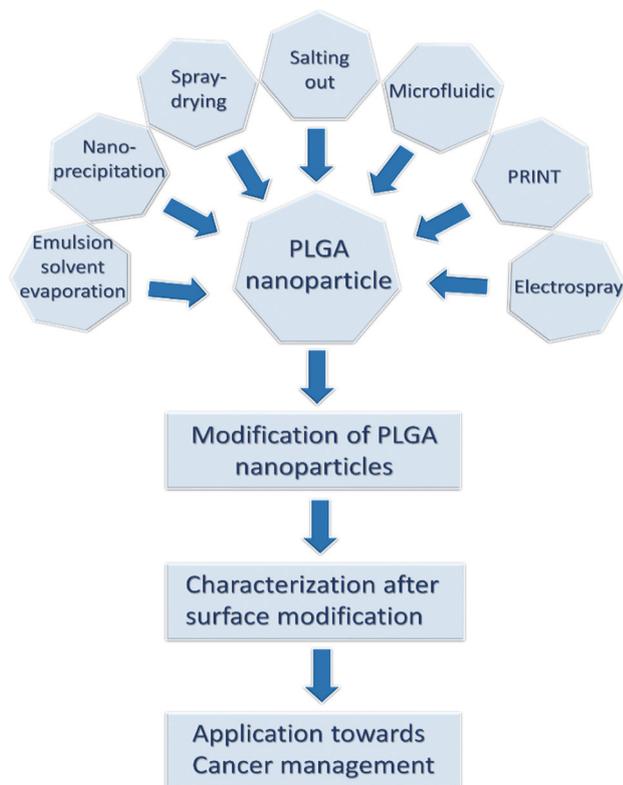

Fig. 1   The review's structure based on PLGA nano-carrier formulation, surface modification, and cancer therapeutic applications.
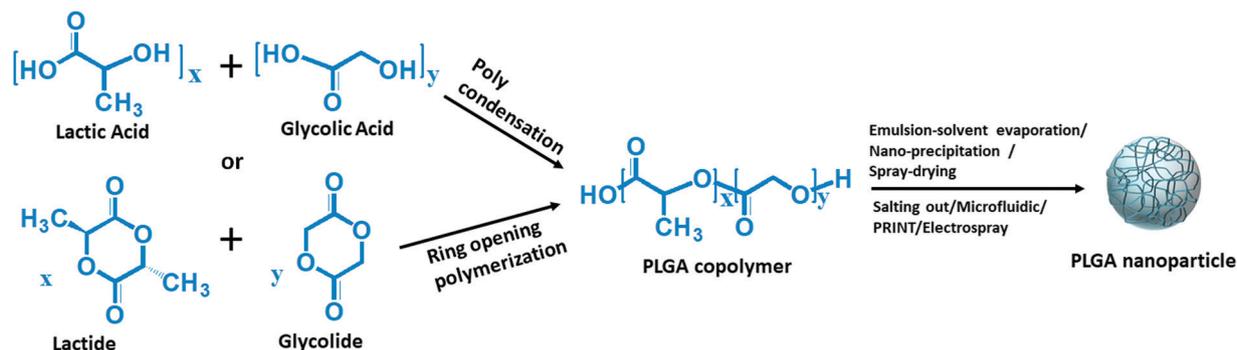
Fig. 2 Reaction mechanism for the formation of PLGA nanoparticles.

emulsion step (Fig. 3). A single emulsion step is required for the encapsulation of hydrophobic molecules, whereas double emulsion steps are required for the encapsulation of hydrophilic molecules.

In the single emulsion solvent evaporation method, both PLGA and hydrophobic drugs are dissolved in a non-polar organic solvent, which is then added drop-wise to the aqueous solution of surfactants (stabilizers) with continuous agitation (ultra-sonication or homogenization). The high shear stress disperses the oil–water emulsion into nanoparticles, which hardens after evaporation of the organic solvent by continuous stirring (Fig. 3a).[56,57] For the encapsulation of hydrophilic drugs, the PLGA solution is drop-wise added to the aqueous drug solution with continuous stirring that produces the first emulsion. Then, the first emulsion is transferred to the

Table 2 The process parameters, key characteristics, advantages, and limitations of the PLGA nanoparticles synthesis

| Name of the method	Parameters that affect nano-particles size	LA:GA and size of nano-particles (nm)	Drug loading (%) and encapsulation efficiency (%)	Advantages	Limitations	Ref.
Conventional methods						
Emulsion-solvent evaporation	Polymer concentration, speed of agitation, stabilizer concentration	50:50, 75:25, 85:15; and 100–500	0.022–8 and 20–80	Spherical morphology, easy and rapid procedure of nano-particle fabrication, colloidal stability	Heterogeneous in size, residual stabilizer remains, particle agglomeration, drugs may lose activity due to high shear stress	52–57,59,60
Nano-precipitation	Polymer concentration, speed of agitation, stabilizer concentration	50:50, 75:25, 85:15; and 50–300	1.7–10 and 40–90	High yield, easy and reproducible	High polydispersity index, use of stabilizer, high speed agitation may degrade drug molecules	61–66
Spray-drying	Spray mesh hole size, concentration of the polymer, density of the spray liquid, flow rate	50:50, 75:25; and > 300	1.5–7.4 and 65–90	It produced powder nano-particles, stable in storage because free of moisture, nanoparticles produced free from contamination of other chemicals	Degradation of the temperature sensitive drug due to the high heat, high operating cost, and agglomeration of nanoparticles	67–73
Salting out	Polymer concentration, stirring speed, stabilizer concentration, concentration of salting out agent	50:50, 75:25; and 55–500	5 and 55–80	Use of nontoxic oil phase, nanoparticles size can be controlled by adjusting different parameters	Purifying the nanoparticles is very hectic due to the presence of salting out agent, high speed agitation may result in loss of drug activity	74–76
Nonconventional methods						
Microfluidic	Channel geometry, flow rate ratio of the continuous phase and dispersed phase, inter-facial tension between two phases, Mixing time	50:50, 75:25; and 40–200	10–18 and ∼90%	Narrow size distribution, reproducible	Swelling of PDMS polymer alters channel geometry, very low yield	77–80
PRINT	Template patterns, mold preparation	50:50, 85:15; and 10–300	1–40 and > 90%	Monodispersed particle, high encapsulation efficiency, reproducible	Low yield, degradation of clinically important fragile molecules during solidification	81–86
Electrospray	Concentration of the polymer, nature of solvent, needle diameter flow rate, potential difference and distance between needle and grounded electrode	50:50 and 10–500	5–43 and > 90%	High yield in a short duration of time, single step method, surfactant and high speed agitation free process		87–89
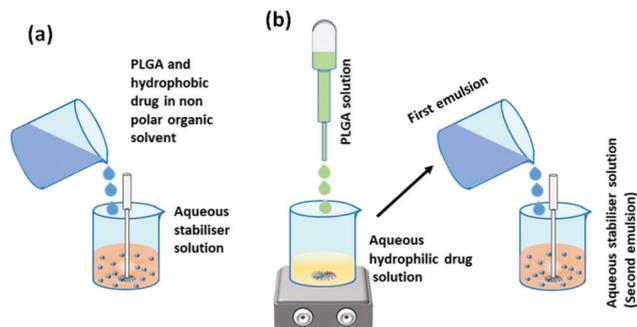
Fig. 3 Synthesis of PLGA nanoparticles by (a) single emulsion-solvent evaporation method and (b) double emulsion solvent evaporation method.

aqueous solution of surfactants (water in oil in water) under ultra-sonication or homogenization, which forms the second emulsion that finally transforms into the hydrophilic drug encapsulated PLGA nanoparticles (Fig. 3b).[55,57] The nanoparticles are solidified after the evaporation step like the single emulsion method. The vigorous mechanical agitation step in the stabilizer containing aqueous medium disperses the emulsion into nano-droplets of varying sizes with a layer of the stabilizer surrounding it. Nanoparticle size increases with the increase in PLGA concentration. At higher PLGA concentrations, the viscosity of the organic phase obstructs the disruption of the emulsion into very small-sized nano-droplets; as a result, a high number of PLGA polymer resides in the droplet, which eventually produces nanoparticles with a larger size.[58,59] Manchanda et al. reported that a higher concentration of the stabilizer in an aqueous medium increases the overall shear force on the emulsion droplets by reducing the organic/aqueous interfacial tension, which eventually helps the formation of nanoparticles with a smaller mean diameter. They also reported that the drug encapsulation efficiency increases with the increase in PLGA concentration as high viscosity resists the diffusion of the drug into the aqueous medium. A high polymer ratio also provides a dense network to trap the drug molecules.[60] The agitation speed also has a remarkable effect on the size of the nanoparticles. The high agitation speed produces smaller nanoparticles by rupturing the emulsion droplets into smaller ones containing lesser PLGA polymer. Kadriye Kizilbey conducted a series of experiments to optimize the parameters to encapsulate hydrophobic drugs inside PLGA nanoparticles using the single emulsion solvent evaporation method. He reported that the diameter and encapsulation efficiency of nanoparticles increase with the increase in PLGA concentration. At the same time, the increasing concentration of PVA (stabilizer) has a similar effect on size but has a reverse effect on encapsulation efficiency.[56]

2.1.2 Nano-precipitation method. This procedure is mainly used for the synthesis of hydrophobic molecule encapsulated PLGA nanoparticles. The encapsulation efficiency of the hydrophilic drug is low because of its propensity to diffuse towards the aqueous phase from the organic phase during rapid intermixing and evaporation of the organic solvent.[61] Nano-precipitation is a one-step process in which water-miscible organic solvent containing PLGA and the hydrophobic

drug is slowly added through a syringe pump to an aqueous solution with high speed agitation (Fig. 4).[62–64] The organic phase diffuses very fast into the aqueous phase, which helps rapid precipitation of the nanoparticles encapsulating a high amount of the drug in its hydrophobic core.[61] The rapidly collapsed PLGA nanoparticles become solid after the complete evaporation of the organic phase. The nanoparticle formation is going through three stages i.e. supersaturation, nucleation, and growth. In the beginning, local supersaturation of the polymer solution at the interface of the organic solution and aqueous phase through the high-speed turbulence provides a driving force for the nucleation of the polymer. At that critical saturation level, a large quantity of small nuclei is formed. Then, the concentration of the polymer solution (at the interface of local supersaturation) drops, which becomes unfavorable for further nuclei formation. The nuclei are then grown by adding polymer molecules one by one until the polymer solution reaches equilibrium.[58,63–65] Faster nucleation rate results in smaller sized nanoparticles.[64] The nanoparticle's size increases with the increasing concentration of PLGA solution due to the viscosity and the supersaturation phenomenon.[66] Unlike the emulsification technique, the nanoparticle's diameter increases with the increasing concentration of the stabilizer.[58] The high encapsulation efficiency of hydrophobic drugs can be achieved using this procedure because high speed mixing of the solvent into anti-solvent helps rapid collapse of the PLGA nanoparticles by encapsulating the drug molecules inside its hydrophobic core.

2.1.3 Spray-drying method. This is a one-step powder nanoparticle synthesis process from solution and emulsion using a nano-spray dryer. The polymer–drug emulsion is atomized by ejecting through a mesh of precisely narrow-sized holes (∼4–7 μm) using vibration mesh technology into a laminar flow of drying hot gas chamber (nitrogen and carbon dioxide at ∼45–60 °C). The dried particles are collected in an electrostatic particle collector by inducing the charge on the dry particle surface (Fig. 5). Hot drying gas is required to transform the tiny droplets into completely dry particles by evaporating the solvent and then exhausting the gas in air through a filter after reducing
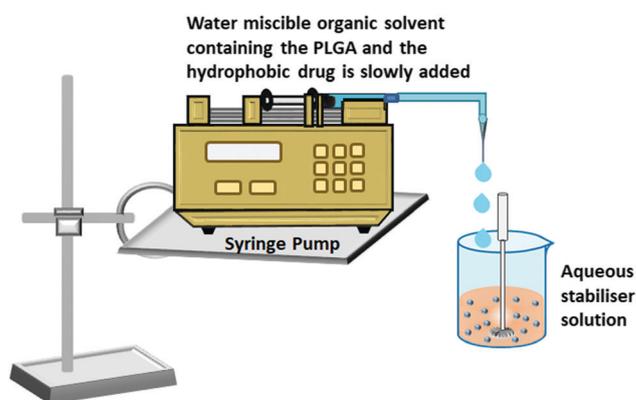

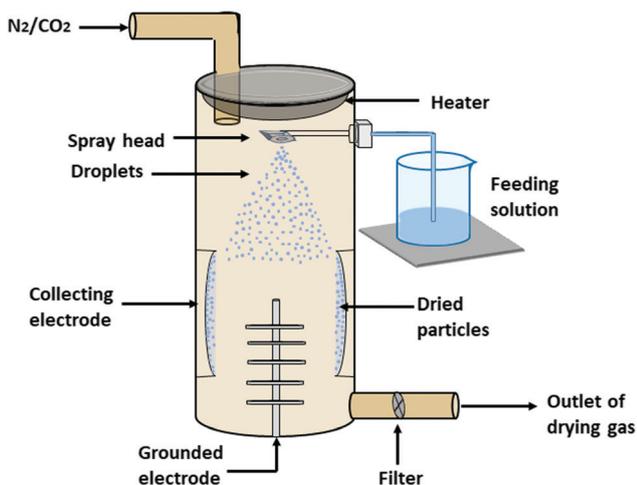Fig. 4 Synthesis of PLGA nanoparticles by the nano-precipitation method.

Fig. 5 Synthesis of PLGA nanoparticles by spray-drying method.

the gas temperature to ~25–30 °C.[67–70] Both the hydrophobic and hydrophilic molecules can be encapsulated in PLGA nanoparticles using this process by feeding the single and double PLGA-drug emulsion, respectively, in the spray head. The size of the particles is controlled by the spray mesh hole size and concentration of the polymer. Particle size increases with the increase of the spray mesh hole size and concentration of the polymer. The density of the spray liquid and the flow rate has a significant impact on the particle size.[71] This procedure was used by Kohl et al. to synthesize photoacoustic contrast agent (near-infrared dyes) encapsulated PLGA nanoparticles with a broad size range 540–255 nm. They have shown efficiency in diagnostic applications on human hepatocarcinoma cells and monkey kidney cells. They used gas inlet temperature range of 47°–52 °C, gas outlet temperature range of 25°–30 °C, and PLGA-dye solution feeding rate 5.5–6 mL min^{-1}.[68] Jensen et al. mentioned their optimized parameters for the synthesis of carbohydrate stabilized siRNA loaded PLGA nanocomposite containing microparticles. The aqueous carbohydrate solution suspending siRNA loaded PLGA nanoparticles was used for the spray drying synthesis of the particles to pulmonary delivery of siRNA. The optimized parameters include suspension feed rate of 0.3 mL min^{-1}, inlet temperature of 45 °C, and outlet temperature of 30 °C to synthesize this delivery vehicle.[69] Panda et al. reported the synthesis of hydrophobic antipsychotic drugs clozapine (CLZ) and risperidone (RIS) co-encapsulated in PLGA nanoparticles from the emulsion of PLGA-drugs using spray drying method and the applied parameters were, feed rate 2 mL min^{-1}, inlet temperature 60 °C, and outlet temperature 31 °C.[70] With this method, many authors reported high encapsulation efficiency, which is comparable with the previously described methods. The nanoparticles' lifespan and entrapped molecules are extended due to the complete dehydration of the nanoparticles during the spray drying synthesis, which finally produces nanoparticles in powdered form.[72] The drawbacks of the method are agglomeration and loss of the nanoparticles as it sticks on the electrostatic particle collector wall and the high drying gas temperature may degrade the heat sensitive drug molecules. At this high

temperature, the PLGA structure can be damaged because the glass transition temperature of PLGA is in the range of 40–60 °C.[34]

2.1.4 Salting out method. The salt-induced precipitation concept is used in this drug encapsulated nanoparticle synthesis method. In this method, the PLGA and hydrophobic molecules are dissolved in a water-miscible organic solvent, which is added to the aqueous phase containing the stabilizer and concentrated salting-out agent (electrolytes like magnesium chloride, calcium chloride, magnesium acetate, and non-electrolytes like sucrose) under stirring to produce nano-droplets from the oil–water emulsion (Fig. 6). The high concentration of the salting-out agents hinders the miscibility of the organic phase with the aqueous phase by attracting and surrounding itself with water molecules. However, when the excess amount of water is added to the system, the organic solvent starts to rapidly mix with the aqueous phase, which creates an interfacial turbulence. As the solvent diffuses from the nano-droplets, the polymer is squeezed to form nanoparticles and stabilized by the stabilizer molecules.[73] Nanoparticles are collected by cross-flow filtration. Parameters of this method influence the nanoparticle's size in a similar way as emulsion solvent evaporation and nanoprecipitation methods. With an increase in PLGA concentration after an optimum level, the density of the oil phase increases, which reduces the net shear stress during emulsification. Thus, it is unable to produce smaller-sized droplets and eventually leads to the formation of larger-sized particles.[74–76] The higher concentration of the stabilizer reduces the oil–water interfacial tension; as a result, the net shear stress is increased significantly, which efficiently forms smaller droplets and then eventually produces nanoparticles with smaller mean diameter after complete diffusion of the solvent.[74–76] The nanoparticles' size was reduced with the increased speed of agitation and decreased electrolyte concentration.[75,76] The dependency of the encapsulation efficiency on the process parameters was studied by Song et al. They stated that encapsulation efficiency increases with the increasing concentration of PLGA and salting-out agents. However, encapsulation efficiency reduces with the increase in stabilizer concentration.[75]

2.2 Nonconventional approaches

Nowadays, various interdisciplinary approaches have been introduced to overcome several limitations like multi-step
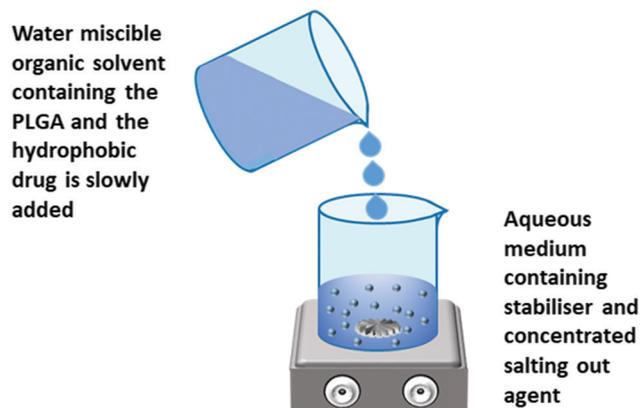

Fig. 6 Synthesis of PLGA nanoparticles by salting out method.

synthesis process, reduced drug loading, low yield, polydispersity in size, and the involvement of biohazard materials. Conventional ways of PLGA nanoparticle synthesis are emulsion-solvent evaporation, nano-precipitation, salting out, and spray-drying methods. These methods usually employ more than one solvent phase with stabilizer/cross-linker and high shear stress for a prolonged time, resulting in polydispersity in the nanoparticle size. Nevertheless, after several washes of the synthesized nanoparticles, some residual solvent may remain, which may result in undesirable toxic effects in the application phase.

2.2.1 Microfluidic method. Microfluidics is a newly evolved complete setup to conduct tissue engineering, various biochemical analyses, and controlled synthesis of nanomaterials within a sub-millimetre range capillary network. It is a micro-scale technique used recently to synthesize nanoparticles by utilizing fluid behavior inside a microchannel system. The microfluidic channel is fabricated by polymers (polydimethyl-siloxane (PDMS), polyimide), aluminium, and glass capillaries in which fluid flows in a laminar fashion.[77] The microfluidic flow is generally single-phase and the two-phase flow is inside the channel. The two-phase flow is used to synthesize nanoparticles due to its various advantages, like increasing the interfacial area, reducing the mass-transfer distance, and enhancing the mixing efficiency. The two-phase flow of the microfluidic nanoparticle synthesis method can be categorized into droplet-based and continuous microfluidics-based, depending on the reaction fluid's flow property. In droplet-based microfluidics, the instability between two immiscible phases is the continuous phase and dispersed phase, generated by passive and active techniques that produce uniform and monodispersed droplets. The passive droplet formation is simpler than an active method because external energy, *i.e.*, electrical, magnetic, centrifugal force, is required in the second case. The formation of droplets is controlled by the channel geometry, flow rate, fluid viscosity, and surfactant. Channel geometry of the droplet-based method is mainly three types: cross-flow, flow-focusing, and co-flow (Fig. 7). In cross-flow geometry, the channel shape looks like "T" with the continuous phase flowing through two horizontal inlets and the dispersed phase flowing through a perpendicular inlet. In the flow-focusing method, the dispersed phase flows through a straight narrow channel, and the continuous phase flows through the anti-parallel of the dispersed flow from both sides. In the co-flow process, the dispersed phase flows coaxially with the continuous phase. In continuous microfluidics, two or more fluids flow parallelly inside channels without the formation of droplets.[77,78] Among all the materials used to
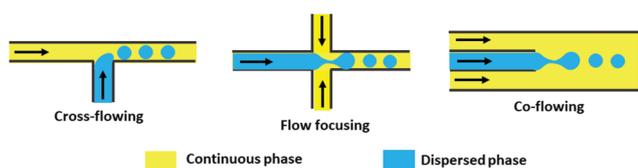
fabricate microfluidic reactors, PDMS is the most commonly used as it is transparent, easy to fabricate, and chemically inert with most of the solvents.[79] However, some of the solvents frequently used to synthesize PLGA nanoparticles react with PDMS and swell the channel, disrupting the reproducibility of the nanoparticle synthesis by altering the channel width. To address this limitation of PDMS microchannels, Mahmoodi *et al.* fabricated a T-junction microfluidic chip with three inlets and one outlet using PDMS for the synthesis of dexamethasone encapsulated PLGA nanoparticles and modified the channel surface with a layer of polytetrafluoroethylene (PTFE) nanoparticles to prevent the absorption and adhesion of the solvent in the PDMS wall. PTFE nanoparticle coating makes the channel super-hydrophobic by increasing the contact angle from $59.37°$ to $140.3°$. They observed that the nanoparticle's size increases with an increase in the mixing time of the PLGA-dexamethasone solution in methylene chloride and water.[80]

2.2.2 Particle replication in non-wetting template (PRINT) method. This is a soft lithography technique developed by DeSimone and his research group. In this technique, pre-defined patterns of desired nanoparticle's size and shape are fabricated on a silicon wafer by the photolithography technique.[81] The patterned silicon wafer is used as a master template in the succeeding synthesis process. A chemically resistant liquid perfluoropolyether elastomer is used to imprint the pattern of the master template and photo-cured to generate the mold. Due to the low surface energy, it is nonwetting in nature, eliminating "scum" formation and making it easy to remove intact solid nanoparticles from the mold cavity.[81,82] The PLGA solution is then poured inside a nano-sized mold cavity using the roll-to-roll technique and solidified after solvent evaporation. The mold containing solid PLGA nanoparticles is then flipped on a high-energy adhesive aqueous soluble harvesting film under the influence of heat and pressure.[83] Then, the nanoparticles are entirely pulled out of the harvesting film and collected in an aqueous medium by dissolving the film (Fig. 8). In this procedure, great control over the parameters produced monodispersed nanoparticles with desirable shape and size.[84] Encapsulation of various biomolecules, including hydrophobic and hydrophilic molecules with negligible loss

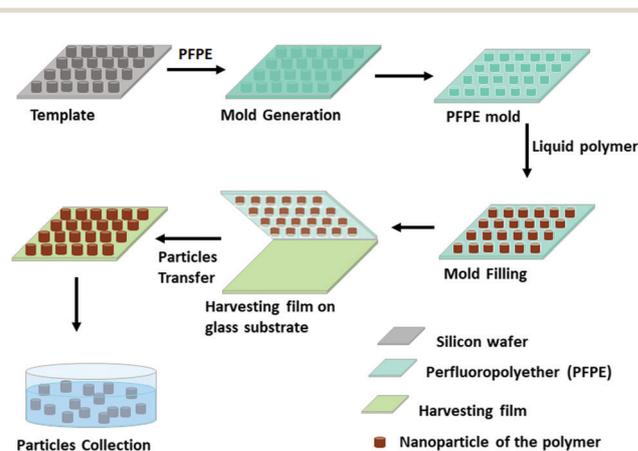**Fig. 7** Synthesis of PLGA nanoparticles by microfluidic method.

Fig. 8 Synthesis of PLGA nanoparticles by PRINT method.

during nanoparticle formation, significantly increases encapsulation efficiency. This is proved by Enlow et al. in their work where they synthesized PLGA nanoparticles with homogeneous size distribution having 40% drug loading and greater than 90% encapsulation efficiency.[82] This method was used by Hasan et al. to encapsulate siRNA inside PLGA nanoparticles and delivered to knockdown genes related to prostate cancer.[85] Chu et al. synthesized docetaxel loaded cylindrical shaped PLGA nanoparticles that are PRINT-Doc-80 × 320 (diameter = 80 nm and height = 320 nm) and PRINT-Doc-200 × 200 (diameter = 200 nm and height = 200 nm) by the PRINT method with very high drug loading. They compared the pharmacokinetics behavior and bio-distribution between both particles depending on their size and shape in mice bearing human ovarian carcinoma SKOV-3 flank xenografts.[86]

2.2.3 Electrospray method. This method's working principle is that a high electric potential applied to the droplets of the polymer solution ejected through a conductive needle makes it a charged entity that deforms and eventually ruptures into charged nanoscale droplets (Fig. 9). The applied voltage acts as an electrostatic force on the droplet (Coulomb force) and competes with the droplet's intrinsic cohesive force (exhibited as surface tension). The gradual increase of the applied voltage initiates charge accumulation on the droplet surface, which produces electric stress leading to the formation of conical shaped Taylor cone at the junction of the needle and droplet. At a certain voltage, the accumulated charge in the droplet exceeds the optimum capacity limit due to the progressive shrinkage of the droplet caused by continuous solvent evaporation, known as the Rayleigh limit. When the Rayleigh limit is reached, the Coulomb force overcomes the cohesive force and the charged droplet is ruptured at the Taylor cone into a cloud of fine nano-droplets, which is called Rayleigh disintegration or coulomb fission. The offspring nano-droplets become solid nanoparticles due to the evaporation of the solvent during the flight before they reach the collector (Fig. 9).[87–91] The electrospray process is operated inside a closed chamber to avoid external disturbances like dirt, airflow, and humidity. The formation of nanoparticles in this method depends on parameters like concentration of the polymer, nature of the solvent, constant flow rate, needle diameter,

stable voltage (above the Rayleigh limit), and a fixed distance between the needle and grounded collector, which are controllable and can be fine-tuned as per requirement. These parameters have an interdependent impact on the fabrication of homogeneous nanoparticles by electrospraying.

Every type of polymer with a specific molecular weight has a particular number of chain entanglements in a specific type of solvent, which increases with the increasing polymer concentration. As the concentration of the polymer increases, the viscosity of the polymer solution gets enhanced, producing a higher chain entanglement density that is physical overlapping of the polymer chain. Above the critical chain overlap concentration, the electrospinning that is fiber formation begins by inhibiting Rayleigh disintegration of the droplets. Polymer concentration below the critical chain overlap concentration favors electrospraying. A lower PLGA concentration decreases the nanoparticle's size as there is no or low chain entanglement in the solution.[88] The solvent should be highly volatile and conductive in electrospray-mediated polymer nanoparticle synthesis. During the flight of the nano-droplets, the whole solvent must completely evaporate before reaching the collector.[88] A specific flow rate of the spray solution through the conductive needle is indispensable to get a stable spray for nanoparticle formation. For the synthesis of monodispersed nanoparticles, a steady flow with a sufficiently low rate is required. At a high flow rate, an intermittent jet is produced instead of an electrospray. The particle size also depends on the flow rate. Smaller particles are formed from the slower flow rate.[88] Stable electrospraying depends on the needle diameter when the flow rate, applied voltage, and electrospray setup are stable. A smaller needle diameter produces more stable and smaller spherical nanoparticles.[88] The stable coulomb fission can be obtained only above a certain applied voltage at a fixed flow rate and electrospray setup. As the voltage increases, the spray solution's dribbling from the conductive needle starts to be finer and eventually becomes nano-spray.[88] The distance between the conductive needle and the grounded electrode decides the electric field strength, which influences the droplets' rupturing. Shorter distance intensifies the electric field strength, which leads to smaller-sized particle formation when other parameters are fixed. A sufficient distance is also required for the complete evaporation of the solvent. If the distance becomes more, then a higher voltage is required to overcome the spray jet.[88]

3 Modification of PLGA nanoparticles

The clinically important molecules are less efficient to reach and accomplish the desired diagnostic or therapeutic aim solely due to their various unfavorable and adverse effects (hydrophobicity, toxicity, ionic form, and coagulation). Drug delivery systems overcome these limitations by providing a frontier solution to increase the drug molecules' pharmacological efficacy and bioavailability by entrapping the drug molecules inside their core. As PLGA is deficient in functional groups, it is necessary to
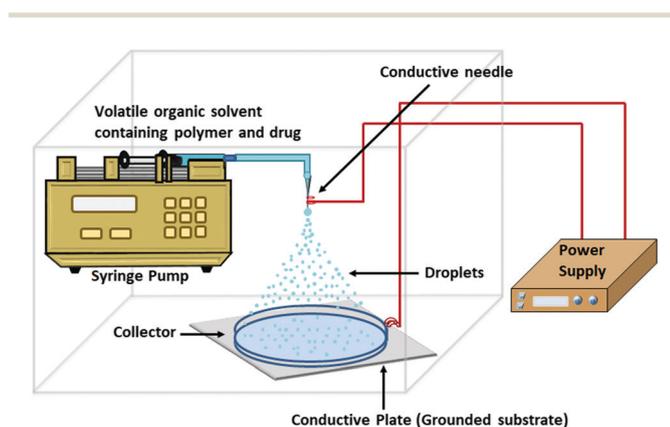

Fig. 9 Synthesis of PLGA nanoparticles by electrospray method.

functionalize it with additional functional groups to convey the clinically important molecules at the site where it is required. Modification techniques of PLGA nanoparticles are summarised in Table 3. The modification also provides a high degree of flexibility by altering the polymer and particle surface properties to make it suitable for therapeutic and imaging applications.

3.1 Non-covalent

Non-covalent binding is a reversible interaction that provides easy attachment and detachment of the desired molecules at predefined conditions. This interaction is weak in nature; it includes hydrophobic, hydrogen bonds, and electrostatic interactions (Fig. 10a–c).[92] As there is no stable bond formed between PLGA and ligand, the conjugation is very unstable. When a faster rate of release is needed, this type of conjugation provides an excellent option. This type of conjugation does not hamper the molecular properties of the ligand. Conjugation of biomolecules using this type of weak interaction is a faster one-step process, and additional use of chemical and purification steps can be avoided. However, unlike covalent conjugation, there is a risk of premature release from the nanoparticle's surface. Another frequently used and the most robust non-covalent interaction is the Avidin–Biotin interaction (Fig. 10d).[92,93] In non-covalent interactions, small molecules are randomly conjugated, which sometimes block the group required for receptor-specific interaction. Avidin–Biotin interaction strategy helps to bind each other with high binding affinity.[92,94] Avidin is a basic tetrameric glycoprotein that irreversibly binds with biotin (Vitamin B7) in a wide range of pH and temperature, facilitating the site-specific quantitative conjugation of clinically important small molecules with PLGA polymer as well as nanoparticles.[95] Using avidin–biotin interaction, Sirianni et al. stably conjugated radioactive isotopes F-18 labelled PEGylated biotin ([18F]-fluorobenzylamide-poly(ethylene glycol)4-biotin) with avidin-modified PLGA nanoparticles for efficient delivery and positron emission tomography imaging in intact rat brain.[96] Despite these advantages, some limitations are there, like non-specific binding at physiological pH (due to basic pI and presence of terminal glycoside moiety) and strong irreversible interaction causing difficulty in the release. To avoid these limitations, streptavidin and neutravidin, which are analogs of avidin can more specifically bind with biotin to make the reaction reversible.[92,95] For this reason, biotin analogs like desthiobiotin are also in use.

3.2 Covalent

Covalent conjugation is a stable conjugation procedure that plays a vital role in the stable transportation of clinically important molecules at a predefined location and rate. It employs multiple steps to form a strong bond between PLGA polymer/nanoparticle surface and small ligands that facilitate long circulation and controlled release at the desired position. It lowers the chance to change the inherent molecular property of the conjugated molecules. For the functionalization of PLGA polymer/nanoparticle, three coupling reactions are generally used, such as carbodiimide coupling, thiol-maleimide coupling, and copper–catalyzed azide–alkyne cycloaddition.

Carbodiimide coupling reaction. This process is the most popular to conjugate the activated carboxyl group (–COOH) with the primary amine group by forming a very stable amide bond. The –COOH group of PLGA is activated by carbodiimide coupling agents (1-ethyl-3-(3-dimethylaminopropyl) carbodiimide (EDC) and dicyclohexylcarbodiimide (DCC)) that produces an intermediate compound o-acylisourea.[93,97–100] The primary amine group is readily conjugated with the –COOH group by replacing the intermediate ester through the nucleophilic attack. The o-acylisourea is very unstable and sparingly soluble in an aqueous solution where it is easily hydrolyzed. To overcome the loss due to hydrolysis, an excess amount of carbodiimide is used, which drastically decreases the colloidal stability of the nanoparticles.[93,99,101] N-hydroxysuccinimide (NHS) or Sulfo-NHS can improve the stability of the active intermediate by the formation of NHS-ester, which has better stability than the previous one.[93,98,99] The primary amine group of biomolecules replaces the NHS-ester intermediate by the nucleophilic attack and form an amide bond with PLGA polymer/nanoparticles

Table 3 Types of surface modifications of PLGA nanoparticles

| Type of interaction	Conjugating molecule	Coupling agent	Reaction environment	Type of bond formation	Ref.
Non-covalent					
Hydrophobic	Hydrophobic biomolecules	—	Depends on the conjugating molecule	Hydrophobic	92
Electrostatic	Positively charged biomolecules	—	Depends on the conjugating molecule	Electrostatic	92
Hydrogen bond	Biomolecules with carboxyl, amine and hydroxyl groups	—	Depends on the conjugating molecule	Hydrogen bond	92
Avidin–Biotin	Any type of biomolecules	Avidin and Biotin	Wide range of pH	Protein and ligand	93–95
Covalent					
Carbodiimide coupling reaction	Biomolecules with primary amine group	Carbodiimides	pH < 7.2	Amide bond	91,98–101
Thiol-maleimide coupling reaction	Biomolecules with sulfhydryl or thiol group	Maleimide	pH 6.5–7.5	Thioether bond	106–109
Copper-catalyzed azide–alkyne cycloaddition (CuAAC) reaction	Biomolecules linked with alkyne group	Azide and alkyne	In the presence of copper(I) catalyst at pH 7.2	5-Membered heteroatom ring (1,2,3-triazole)	117,119,121
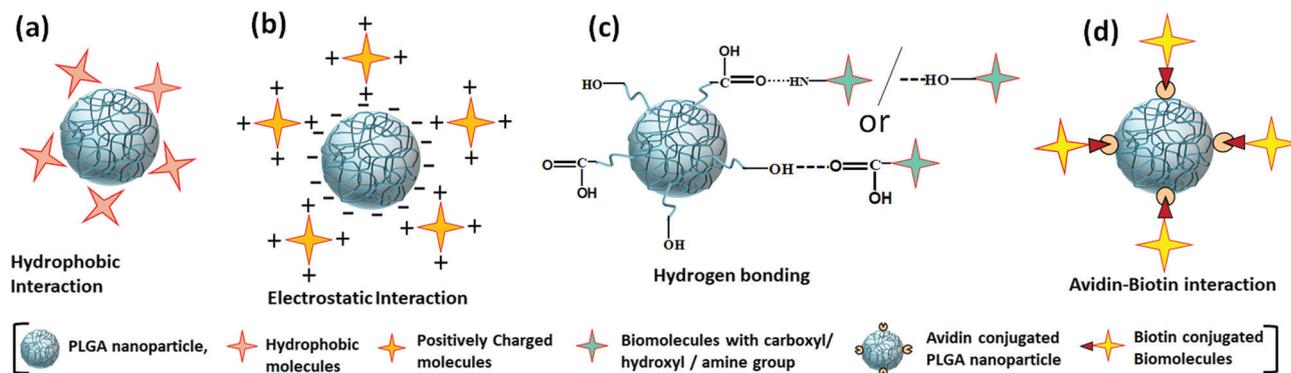
Fig. 10 Non-covalent interactions for the modification of PLGA nanoparticles (a) hydrophobic interaction, (b) electrostatic interaction, (c) hydrogen bonding, (d) avidin–biotin interaction.

(Fig. 11a).[91,98,99,102] Since there is no chemical modification of the biomolecules, it minimizes the chance of loss of activity. This coupling reaction is extensively studied to functionalize PLGA polymer/nanoparticles due to its intrinsic free terminal –COOH groups. Zhang *et al.* used this method to conjugate polyethylene glycol (PEG) on the PLGA nanoparticle's surface to synthesize PEGylated-PLGA nanoparticles. Cyclo(1,12)PenITDGEATDSGC (cLABL) peptide was then conjugated with the –COOH group of PEG oriented outside of the nanoparticles and applied to target intercellular cell-adhesion molecule-1 (ICAM-1) that is overexpressed at inflammatory sites.[103] Graf *et al.* synthesized PLGA-*block*-polyethylene glycol (PLGA-PEG) copolymer using the carbodiimide coupling reaction to synthesize PLGA-PEG nanoparticles by encapsulating cisplatin prodrug (Pt(hex)2) inside its hydrophobic core, which makes the carboxyl group of the

hydrophilic PEG available on the nanoparticle's surface. The cyclic pentapeptide c(RGDfK) was conjugated with the carboxyl group of the PEG using EDC/NHS coupling to specifically target αvβ3 integrins, which are upregulated on angiogenic endothelial cells.[104] Liu *et al.* synthesized PLGA-PEG copolymer from PEG bis-amine to achieve free primary amine group decorated PLGA-PEG/PLGA nanoparticle surface. Carboxyl end of the herceptin antibody conjugated with the primary amine group of PEG and another amino-terminal end remains free for targeting HER2 receptor expressed on the SK-BR-3 and MCF7 breast cancer cells.[105]

Thiol-maleimide coupling reaction. This is a type of Michael addition reaction that is efficient in selective conjugation of sulfhydryl or thiol group containing biomolecules.[93,106,107] Maleimide is a thiol reactive compound that specifically forms
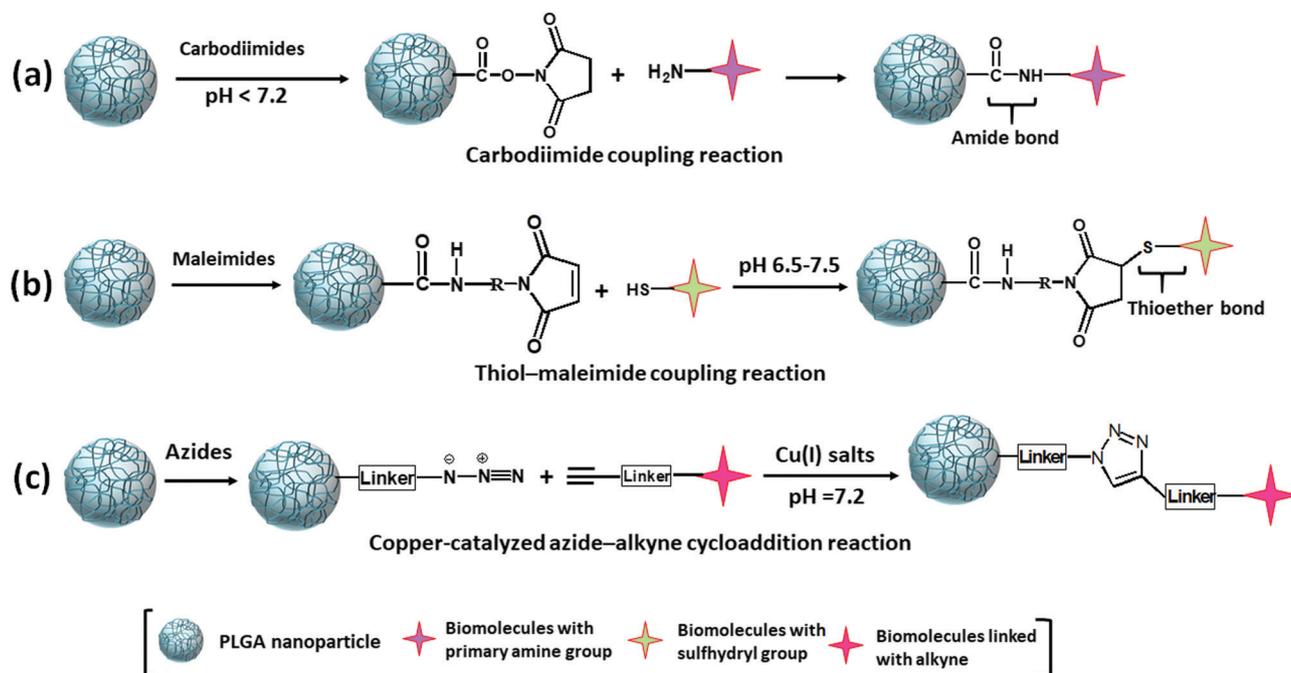

Fig. 11 Covalent modification of PLGA nanoparticles by (a) carbodiimide coupling, (b) thiol-maleimide coupling, (c) copper-catalyzed azide–alkyne cycloaddition reactions.

a stable thioether bond with the thiol group at natural pH (Fig. 11b).[107,108] Since this group is not abundant like the amine group in molecules, it can more site-specifically bind with free –SH. However, the oxidized form of the thiol group (disulfide bonds in the tertiary structure of proteins and antibodies) remains unreacted, which provides control on the number of binding sites and does not modify the structure as well as biological activity.[107] The thiol group can be created by reducing native disulfide bonds or reacting with the primary amine group using sulfhydryl-addition reagents (2-Iminothiolane (Traut's reagent) and N-succinimidyl S-acetylthioacetate (SATA)). This process introduces heterobifunctional crosslinker in those molecules in which the reactive thiol group is either deficient or unavailable.[93,109] To modify PLGA using this coupling method, the maleimide group first conjugated with the PLGA polymer/nanoparticles *via* linker molecules, then the thiol group containing molecules conjugated with the maleimide group forming thioether bond by the nucleophilic attack (Fig. 11b). Most of the time, maleimide-PEG-amine (H$_2$N-PEG-Mal) is used as a linker molecule and conjugated by the carbodiimide coupling reaction.[93,110] Vasconcelos *et al.* functionalized both the PLGA polymer and nanoparticles with the maleimide group by conjugating H$_2$N-PEG-Mal using EDC/NHS coupling reaction. Then, two different cell-penetrating peptides (human immuno-deficiency virus transactivator protein (HIV-Tat) and peptide for ocular delivery (POD)) were conjugated with the maleimide group by the formation of the thioether bond *via* the thiol group containing cysteine residue of the peptides to study the improvement in corneal epithelium penetration during the ocular delivery of the nonsteroidal anti-inflammatory drug.[111] Conjugation through the thiol group instead of the primary amine group is beneficial, especially for the protein and anti-body. Their amino-terminal domain generally binds with the ligand/receptor, required to be free for their activity. In addition, these clinically important biomolecules naturally possess cysteine residues having thiol groups in free or in disulfide form.[108,112] Similarly, Paka *et al.* Conjugated glutathione (a tripeptide containing free thiol group at the cysteine residue) with the free maleimide group at the terminal distal ends of the crosslinker of PLGA-PEG-Mal nanoparticles to study the betterment of curcumin delivery efficacy by glutathione functionalization.[113] Likewise, Kennedy *et al.* used re-engineered AbD15179 antigen-binding fragment (specifically bind with human CD44v6 glycoprotein overexpressed in metastatic cancers of the epithelium) expressing three cysteine residues near the C-terminus for coupling with the PEG-maleimide functionalized PLGA nanoparticles.[114]

Copper-catalyzed azide–alkyne cycloaddition (CuAAC) reaction. Copper(I)-catalyzed Huisgen 1,3-dipolar cycloaddition reaction between an azide and an alkyne group was discovered by the research groups of Meldal and Sharpless in 2002.[115,116] It is a member of the click chemistry reaction category as it manifests some features of this category like (i) regiospecificity and stereospecificity, (ii) there is no or negligible reaction by-product, (iii) mild reaction conditions, (iv) wide reaction scope with high yield, (v) equally efficient in carrying out the

reaction in aqueous as well as in organic medium.[93,117–120] These properties are useful for the conjugation of biomolecules, which gradually made the CuAAC reaction attractive as a conjugation method for various biomolecules with PLGA. Precise interaction between the azide and an alkyne group eliminates the risk of nonspecific conjugation. The mild reaction condition helps to retain the structural and functional integrity of biomolecules.[117,119] Azide and alkyne groups are pre-conjugated with either PLGA or conjugating biomolecules. Then, they are covalently conjugated by the formation of a 5-membered heteroatom ring (1,2,3-triazole) in the presence of copper(I) catalyst (generated from Cu(I) salts or Cu(II) salts using sodium ascorbate as the reducing agent) through cycloaddition reaction between azide and alkyne groups (Fig. 11c).[119,121] In most conjugations, the azide group is attached with PLGA polymer/nanoparticles *via* linker molecules. The alkyne group is either inherently present or attached with biomolecules through a linker molecule. Saeed *et al.* synthesized folate-conjugated PLGA-S-S-PEGMA475 diblock copolymers using the CuAAC reaction between azide terminated PLGA-S-S-PEGMA475, synthesized *via* nucleophilic substitution and alkyne terminated folic acid synthesized by propargylamine *via* carbodiimide coupling. Finally, plasmid DNA encapsulated and folate receptor-targeted nanoparticle was synthesized using PLGA–S–S–PLGA copolymer and folate-terminated PLGA-S-S-PEGMA475 copolymer for target-specific gene delivery in Calu-3 cell line.[122] Whereas Zhou *et al.* synthesized doxorubicin encapsulated nanoparticle using a tri-block copolymer ((PLGA)-*b*-poly(L-histidine) (PHis)-*b*-polyethylene glycol (PEG) (PLGA-*b*-PHis-*b*-PEG-azide)) conjugated with azide at the hydrophilic PEG end, which helps to orient the azide group on the nanoparticle surface. Then, the alkyne group containing herceptin antibody (the alkyne group was introduced in herceptin antibody *via* NHS-PEG-propargyl linker) was covalently conjugated with the azide group on the nanoparticle surface by the CuAAC reaction to study the pH-sensitive targeted drug delivery efficacy in HER2 receptor overexpressed human breast cancer cell lines.[123] The main drawback of this conjugation method is the presence of the residual copper-based catalyst that remains even after purification and causes cellular toxicity. Another drawback is the use of sodium ascorbate with copper generated reactive oxygen species, which is detrimental for bio-conjugation with the polymer. The by-products of ascorbate can also form an aggregate of proteins by covalent modification.[93,117]

4 Characterizations of PLGA nano-carriers after surface modification

It is necessary to perceive the surface properties of the PLGA nano-carrier after functionalization with desired ligands to get a critical insight into the suitability of therapeutic application. Characteristics of nano-carriers depend on the modification of the PLGA polymer, nanoparticle surface, conjugated molecules, and the type of interaction at the time of conjugation. Intrinsic properties of the nano-carrier like size, charge, shape,

excitation and emission wavelength, molecular composition, and type of bond involved in conjugation are analyzed using various sophisticated analytical methods.[124,125] These physico-chemical properties of the nanoparticle decide the stability, drug encapsulation efficiency, and release kinetics of the nanoparticle, which reflects its applicability as a nano-carrier system. The tuning of the synthesis and functionalization process parameters leads to the modification of the properties of nanoparticles that regulate the behavior of the nanoparticles.[126,127]

Hydrodynamic size and charge of the PLGA nano-carrier are analyzed using a particle size analyzer by the dynamic light scattering technique.[128] The size and charge (Zeta (ζ) potential) are the determining factors to cross the cell-associated barrier for delivering the drug or tracking through an imaging agent.[129] Nano-carrier with size less than 200 nm internalized efficiently by the cell through endocytosis and EPR (enhanced permeability and retention) effect of tumor vasculature. Nanoparticles with a size greater than 200 nm were prematurely eliminated from the body by the reticuloendothelial system (RES).[130,131] A higher ζ potential of PLGA nanoparticles provides colloidal stability of the nanoparticles. The higher surface charge of the nanoparticles produces electrostatic repulsion; thus, they remain suspended in solution, which prevents agglomeration and maintains the size.[132] Nano-particles were analyzed using atomic force microscopy (AFM), field emission scanning electron microscopy (FESEM), and trans-mission electron microscopy (TEM) to study the nanoparticle's shape, increased diameter, and surface texture after surface modification (Fig. 12).[90,91] The nanoparticle's shape and

morphology depend on the synthesis procedure, which has an effect on the cellular uptake of the nanoparticles. A three-dimensional view and line roughness graph of nanoparticles with the sub-nanometer resolution is observed under AFM in atmospheric or submerged conditions.[133] FESEM and TEM analyses also provide information about elemental composition by energy-dispersive X-ray spectroscopy (EDX).[134]

Ultraviolet-visible spectroscopy (UV-vis spectroscopy) is used to study the encapsulated and conjugated ligands/biomolecules in PLGA nano-carriers that absorb light in the UV or visible regions of the electromagnetic spectrum.[135] In a complementary way of UV-vis spectroscopy, fluorescent molecule conjugated PLGA nanoparticles absorb a specific wavelength of light (usually ultraviolet light), then re-emit the light to return from electro-nically excited states to the ground state, which is detected by fluorescence spectroscopy (Fig. 13).[136] These techniques are used to quantify the conjugates present in modified PLGA nano-particles to measure the loading and encapsulation efficiency. The wavelength of maximum absorption (λ_{max}) and maximum emission (λ_{em}) are utilized to study the release kinetics of the drug molecules carried by the PLGA nanoparticles. These optical characteristics help detect, quantify the concentration, and find the level of degradation of the nano-carrier in biological samples.[137]

Elemental characterization provides a deeper understanding of physical, chemical, and biological phenomena of the nano-carrier by the Fourier-transform infrared spectroscopy (FTIR), mass spectroscopy, nuclear magnetic resonance (NMR) spectro-scopy, X-ray photoelectron spectroscopy (XPS), and Raman spectroscopy.[90,91] The most common technique to determine
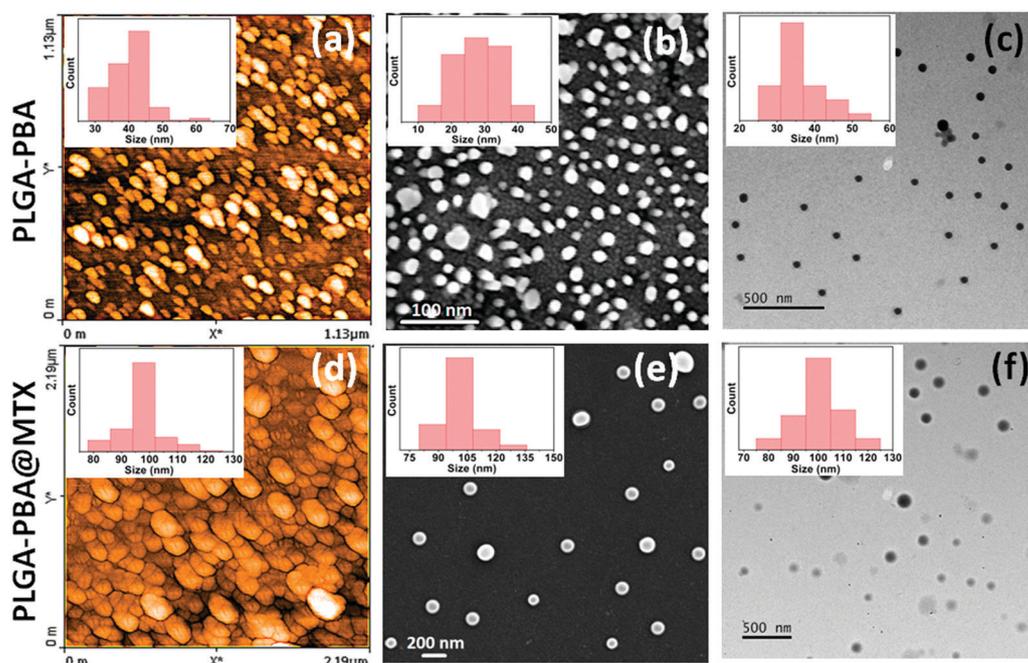
Fig. 12 (a) AFM, (b) FESEM and (c) TEM images of 1-pyrenebutyric acid conjugated PLGA nanoparticles and the same after methotrexate conjugation on the nanoparticles surface through amide linkage shown in (d–f), respectively. The inset shows the corresponding particle size distribution histogram where the increase in particle size establishes the conjugation (Reproduced from ref. 91 with permission from the Royal Society of Chemistry).
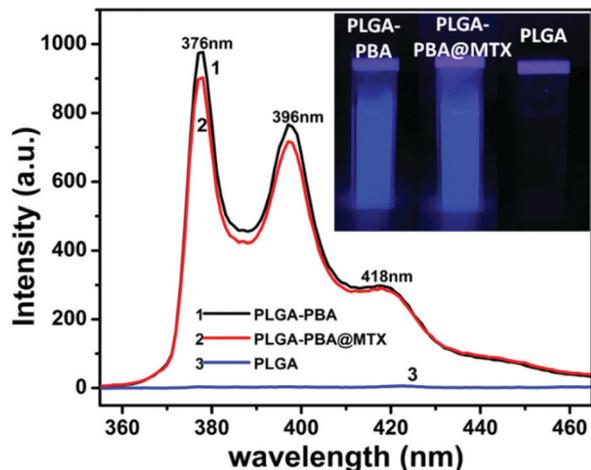
Fig. 13 Fluorescence spectra of PLGA, 1-pyrenebutyric acid (PBA) conjugated PLGA nanoparticles (PLGA-PBA), and methotrexate (MTX) conjugated PLGA-PBA nanoparticles (PLGA-PBA@MTX). The images of nanoparticles suspensions under UV lamp (λ_{max} = 265 nm) are represented in the inset (Reproduced from ref. 91 with permission from the Royal Society of Chemistry).

the elemental composition and type of bonds between the molecules in the nano-carrier by their unique stretching frequencies is FTIR analysis (Fig. 14).[138] The charge to mass ratio of fragmented ions of the nanoparticles during electrospray ionization in the mass spectroscopic analysis technique helps detect the presence of certain molecules and to predict the structure.[139] Proton (^{1}H) and carbon-13 (^{13}C) NMR spectroscopy

are generally used to establish the purity, detect the molecular structure, formation of bonds during conjugation, and analyze the molecules' chemical environment in the nano-conjugate (Fig. 14).[127,135] The chemical state and the electronic state of the elements within the nano-carrier are analyzed using the XPS technique.[135] Raman spectroscopy is employed to analyze the chemical composition and structure of the nano-carrier through a non-contact and non-destructive way by the molecular fingerprint that is the signature vibrational, rotational, and other low-frequency modes of biomolecules.[140]

Analysis of the nano-carrier through all these characterization procedures makes a complete vision about the complete characteristics, which helps determine their mode of effect in further application phases and their limitations.

5 Application of PLGA nanoparticles in cancer

Cancer is one of the fast-growing burdens and also the second leading cause of death around the world.[141] The International Agency for Research on Cancer (IARC) is a part of the world health organization (WHO), which provides an estimation of the global pattern of cancer incidence and mortality in 185 countries for 36 types of cancer in the Globocan database.[142] According to their report in 2018, new cancer cases were 18.1 million, and deaths were 9.6 million, which has risen to 19.3 million new cancer cases and 10 million cancer deaths in 2020 worldwide. They also predict that new cancer cases will be
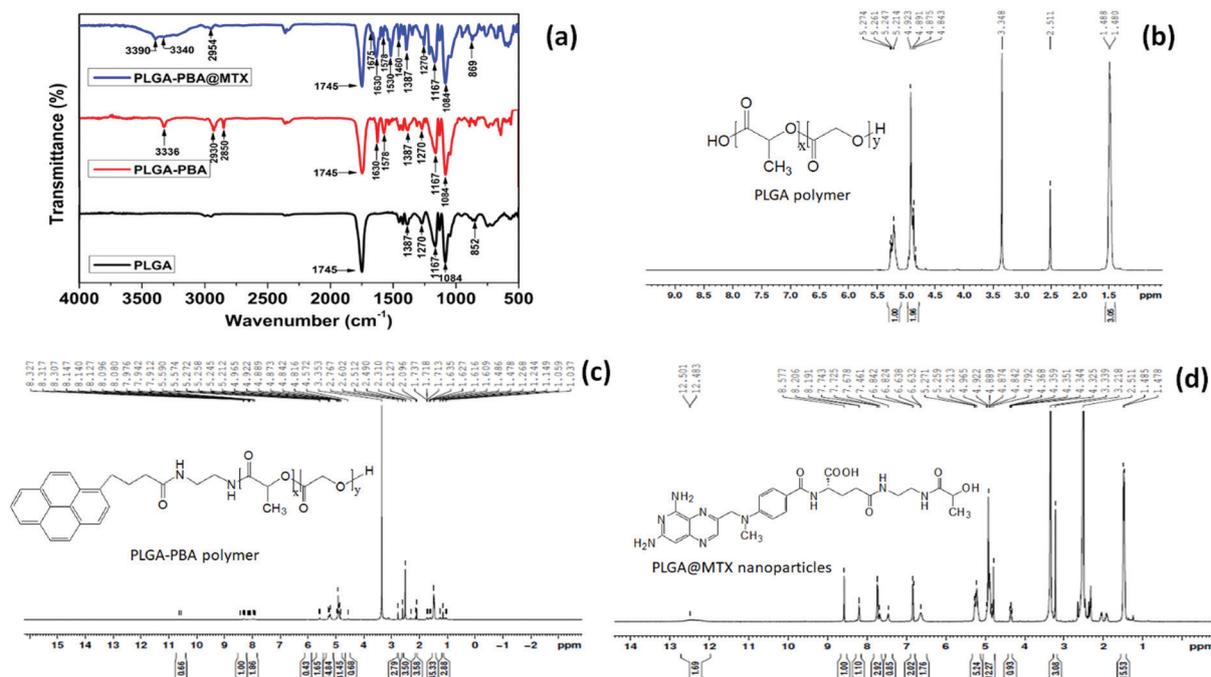
Fig. 14 (a) FTIR spectrum of PLGA polymer, 1-pyrenebutyric acid (PBA) conjugated PLGA polymer (PLGA-PBA) and methotrexate (MTX) conjugated PLGA-PBA nanoparticles (PLGA-PBA@MTX) showing chemical conjugation of PBA and MTX with PLGA before and after nanoparticle formation. ^{1}H NMR analysis of all the conjugation step *i.e.* (b) PLGA polymer (c) PLGA-PBA polymer and (d) PLGA@MTX nanoparticles (Reproduced from ref. 91 with permission from the Royal Society of Chemistry).

29.4 million in 2040.[143–145] According to Globocan 2020, one in five people develop cancer during their lifetime; among them, one in eight men and one in eleven women die due to cancer globally.[144] From the mid of 20th century, typical therapeutic procedures for this lethal disease are radiotherapy, chemotherapy, and surgery.[146,147] In spite of good response, these treatment strategies face diverse challenges such as (i) in radiation therapy, X-ray and γ-ray cause adverse side effects by damaging the nearby healthy tissues, (ii) inadequate drug concentration due to instability in systemic circulation and multi-drug resistance of conventional chemotherapeutic drugs force to increase the therapeutic dose to get an effective concentration of the drug at the disease site that results in adverse side effects, (iii) non-specific bio-distribution produce systemic toxicity, and (iv) limited scope to monitor the administered drug and the treatment response.[148–150] The recent nano-carrier approach of chemotherapy is a revolutionary step that overwhelms the limitations of the usual chemotherapeutic treatment strategy to encounter the increasing rate of cancer.[151–153] Since the last three decades, the application of nanoparticles has been rapidly evolving as a compact platform for efficient drug delivery and monitoring system, along with an increasing understanding of the interaction with the complex biological organization and tumor microenvironment.[146,147]

5.1 Cellular imaging capabilities

Accurate analysis of tumor margin is fundamental for effective therapeutic assessment in pre-treatment and intra-treatment to avoid treatment failure and recurrence of cancer. Xu et al. Developed PLGA nanobubble for intraoperative real-time cancer imaging by the fluorescence and ultrasound method simultaneously. They conjugated HuCC49DCH2 antibody with Texas Red fluorescence dye encapsulated PLGA nanobubble for one-step binding with TAG-72 antigen overexpressed on LS174T human colon cancer cell line. For three-step targeting, biotin conjugated HuCC49DCH2 antibody, streptavidin, and Texas Red encapsulated biotin conjugated PLGA nanobubble were successively applied to the LS174T cells for more accurate targeting.[154] CT and MRI are the common imaging modalities clinically used for the diagnosis and evaluation of therapeutic efficacy. Nowadays, inorganic nanocrystals are frequently used for molecular imaging methods with more specific detection by a high payload of contrast agents. Mieszawska et al. used electron-dense gold nanocrystals (AuNCs), manifesting high X-ray attenuation coefficient and quantum dots (QDs) emitting light in the near infra-red region to integrate with lipid coated PLGA nanoparticles for tunable bio-imaging by computed tomography and fluorescence with high quantum yield.[155] Likewise, for detecting malignancies and monitoring the effects of therapeutic agents using MRI, Mariano et al. synthesized a novel, highly sensitive MRI contrast agent by the entrapment of amphiphilic gadolinium(III) complex (Gd-DOTAMA) in PLGA nanoparticles. The hydrophobic steric chains are confined inside the PLGA core and the hydrophilic Gd coordination cage is partially exposed on the nanoparticle surface, which enhanced the longitudinal relaxation rate in contact with an aqueous solvent that facilitates higher sensitivity in MRI visualization in murine melanoma xenograft.[156] The traveling path of the administered nanoparticles by real-time fluorescence tracking provides excellent control over the therapeutic action and immediate response. To fulfill this purpose, Wang et al. prepared a multifunctional PLGA based nano-platform (PEI-PLGA-PTX-MNPs) by simultaneous encapsulation of super-magnetic γ-Fe_2O_3 nanoparticles (MNPs) and antitumor drug paclitaxel (PTX) inside its core. They also labeled that nanoplatform with polyethyleneimine (PEI)-conjugated fluorescein isothiocyanate (FITC), which is finally applied on human brain glioblastoma U251 cells to study cellular imaging and drug delivery efficacy.[157]

5.2 Drug delivery abilities

PLGA nanoparticles are enormously investigated as a highly effective alternative for the efficient delivery of active therapeutic agents at cancerous tissues by minimizing systemic toxicity. The release rate of anti-proliferative drugs with a high therapeutic payload at the target site from PLGA nano-carriers can be controlled by various formulation processes. The hydrophobic core of PLGA nanoparticles may accommodate various types of drug molecules to transport in a protective manner by prolonging the systemic circulation, which increases the intratumoral accumulation of active therapeutics. One of the major focuses in developing nano-drug delivery systems is to make them target specific to avoid non-specific distribution by conjugating a specific targeting ligand that can strongly bind with the molecules expressed explicitly on the cancerous tissues. The ability of PLGA nano-carriers to cross the leaky tumor vasculature by the EPR effect facilitates passive accumulation at the tumor location. Many research groups are continuously trying to overcome the present treatment challenges by improving the drug delivery process for clinical translation from bench to bedside. Amoozgar et al. developed low molecular-weight chitosan (LMWC) coated PLGA nanoparticles from PLGA-LMWC conjugate, facilitating pH-sensitive cell interaction and encapsulated paclitaxel release inside the weak acidic tumor microenvironment by electrostatic interactions with glycocalyx of the cell membrane. The LMWC surface coating also protects them in systemic circulation from opsonization and phagocytic uptake at neutral pH.[158] Devulapally et al. put their effort to conquer the limitations like tumor recurrence and metastasis of the existing treatment strategy of hepatocellular carcinoma (HCC). The reasons behind the above limitations are intrinsic and acquired drug resistance and low permeability of drugs. They formulated a new drug delivery carrier by the co-encapsulation of antisense-miRNA-21 and gemcitabine (GEM) inside PEGylated-PLGA nanoparticles enhancing the treatment efficacy. The antisense-miRNA-21 downregulates endogenous miRNA-21, which in turn increases the expression of tumor suppressor protein (PTEN) that significantly decreases cell proliferation and increases cytotoxicity in combination with chemotherapeutic drug GEM on the HCC cells.[159] Multi-drug resistant cancer cells show their drug resistance by the efflux of the potent chemotherapeutic drugs like doxorubicin, docetaxel, and paclitaxel. Wu et al. synthesized a novel biocompatible functional surfactant based on amphiphilic vitamin E-oligo(methyl

Table 4 Imaging and drug delivery applications of PLGA nanoparticles in cancer

Nanoparticle formulation	LA:GA and Type of imaging/drug molecules	Synthesis method	Size (nm) and encapsulation efficiency	Application on and administration route	Ref.
Poly(L-lysine)-poly(ethylene glycol)-folate (PLL-PEG-FOL) adsorbed Fe_3O_4 or CdSe/ZnS and DOXO encapsulated PLGA nanoparticle	Fe_3O_4 nanocrystals, CdSe/ZnS nanocrystals and Doxorubicin (DOXO)	Single-emulsion solvent evaporation	100–200;—	KB cancer cells for MR and optical imaging and drug delivery	162
VCR and VRP encapsulated PLGA nanoparticle	75:25; Vincristine (VCR), and verapamil (VRP)	Combining single emulsion solvent evaporation and salting-out method	98.8 ± 8.4; 67.86 ± 5.10% for VCR and 80.29 ± 4.55% for VRP	Multidrug resistant breast cancer cells (MCF-7/ADR) for drug delivery	163
POSS-containing conjugated polymer (CP) loaded and Herceptin conjugated PLGA nanoparticle	50:50; Polyhedral oligomeric silsesquioxanes (POSS)-containing conjugated polymer (CP)	Single-emulsion solvent evaporation	230 ± 3–243 ± 6; 44%	Breast cancer cells (SKBR-3, MCF-7) for optical imaging	164
Herceptin conjugated, Hydrophobic and hydrophilic drugs encapsulated, MNP embedded PLGA nanoparticle	65:35; Magnetic nanoparticles (MNP), paclitaxel (Pac) + rapamycin (Rapa) and paclitaxel (Pac) + carboplatin (Carbo)	Double emulsion solvent evaporation	304 ± 4.1; Pac (80.6 ± 2.7%) + Rapa (86.6 ± 3.1%) and 310 ± 3.9; Pac (83.5 ± 3.0%) + Carbo (47.8 ± 1.5%)	Breast cancer cells (MCF-7), pancreatic cancer cells (PANC-1) and rat model for MR imaging and drug delivery; administered through saphenous vein	165
AS1411 aptamer conjugated and paclitaxel-loaded PLGA nanoparticle	50:50; Paclitaxel	Single-emulsion solvent evaporation	200; —	Human glial cancer cells (GI-1 cells) for drug delivery	166
Curcumin and bortezomib co-encapsulated and alendronate (Aln). conjugated PLGA nanoparticles	50:50; Curcumin and bortezomib	Single-emulsion solvent evaporation	235 ± 70.30; —	Intraosseous mice model of bone metastasis of breast cancer for drug delivery; administered through tail vein	167
Cyclic peptide (cRGD)-modified monomethoxy (polyethylene glycol)-PLGA-poly (L-lysine) nanoparticle encapsulated either DHAQ or Rb	50:50; Mitoxantrone (DHAQ) or rhodamine B (Rb)	Double emulsion solvent evaporation	180; 85.3%	Breast cancer cells (MDA-MB-231) for optical imaging or drug delivery	168
siRNA encapsulated and lipid coated PLGA nanoparticle	Small interfering RNAs (siRNA)	PRINT	207 ± 4.461; 46%	Human cervical (HeLa), prostate (PC3, DU145, LNCaP) and liver (HepG2) cancer cells for siRNA delivery	85
Curcumin loaded PLGA nanoparticles	50:50; Curcumin	Single-emulsion solvent evaporation	120; 80%	Breast cancer cells (MCF7) for drug delivery	169
DOX and VER combined chitosan shell coated MNPs encapsulated and cRGD peptide functionalized PLGA nanoparticle.	50:50; Doxorubicin (DOX), verapamil (VER) and magnetic nanoparticles (MNPs)	Double emulsion solvent evaporation	144; 74.8% for DOX and 53.2% for VER	Male S-180 sarcoma-bearing mice for drug delivery; administered through tail vein	170
Holo-transferrin conjugated and bortezomib-loaded PLGA nanoparticle	50:50; Bortezomib (BTZ)	Single-emulsion solvent evaporation	200; 53 ± 6%	Human pancreatic cancer cells (SUIT-2) for drug delivery	171
DOX encapsulated and low-molecular-weight protamine-surface modified PLGA nanoparticle	Doxorubicin (DOX)	Nanoprecipitation	206.2; 83%	Mice harboring drug-resistant breast tumors for drug delivery; administered through tail vein	172
Tam encapsulated herceptin conjugated polyvinyl-pyrrolidone coated PLGA nanoparticle	50:50; Tamoxifen (Tam)	Double emulsion solvent evaporation	93.44; 72.4 ± 2.3%	Human breast cancer cells (MCF-7) for drug delivery	173
BSA-Gd complexes and DOX encapsulated and poly(ethylene glycol) conjugated PLGA nanoparticle	Bovine serum albumin gadolinium (BSA-Gd) complexes and Doxorubicin (DOX)	Single-emulsion solvent evaporation	280; 20.9%	Human cervical cancer cells (HeLa) and female nude mice bearing tumor for MR imaging and drug delivery; administered through tail vein	174
SPION, QDs and the anticancer drug busulfan encapsulated PLGA nanoparticle	50:50; Superparamagnetic iron oxide nanoparticles (SPION), manganese-doped zinc sulfide (Mn:ZnS) quantum dots (QDs) and busulfan	Single-emulsion solvent evaporation	93; 89 ± 2%	Murine macrophage cells (J774A) and rat model for MR and optical imaging; administered through intravenous mode	175
Antisense-miR-21 and antisense-miR-10b co-loaded urokinase plasminogen activator receptor (uPAR) conjugated PLGA nanoparticle	50:50; Antisense-miR-21 and antisense-miR-10b	Double emulsion solvent evaporation	100 to 200; 72.4 ± 6.2%	Triple negative breast cancer (TNBC) cells and TNBC tumor xenografts in nude mice for antisense-miRNAs delivery; administered through intravenous mode	176

Table 4   (continued)

Nanoparticle formulation	LA : GA and Type of imaging/ drug molecules	Synthesis method	Size (nm) and encapsulation efficiency	Application on and administration route	Ref.
Nutlin-3a loaded EpCAM aptamer and quantum dots conjugated PLGA nanoparticle	50 : 50; Nutlin-3a	Single-emulsion solvent evaporation	292 ± 10; 51.24 ± 6.7%	Human breast cancer cells (MCF-7 and ZR751) and ovarian cancer cells (SKOV3) for fluorescence imaging and drug delivery	177
T7-peptide conjugate, MNPs, PTX and CUR co-encapsulated PLGA nanoparticle	50 : 50; Iron oxide nanoparticles (MNPs), paclitaxel (PTX) and curcumin (CUR)	Single-emulsion solvent evaporation	130; 68% for PTX and 18% for CUR	Human malignant glioma (U87) and mice bearing orthotopic glioma (U87-Luc) for drug delivery and MRI; administered through tail vein	178
DOX-loaded lipid hybrid PLGA nanoparticles	75 : 25; Doxorubicin (DOX)	Double emulsion solvent evaporation	198 ± 12; 86.4 ± 8.5%	Human breast cancer cells (MDA-MB-231/ADR) and human squamous carcinoma cells (KB) for drug delivery	179
Superparamagnetic iron oxide (SPIO3 NPs4) loaded PLGA nanospheres	Oleic acid-coated superparamagnetic iron oxide (SPIO3 NPs4)	Multiple emulsion solvent evaporation method	130; 90.2 ± 0.3%	T1-weighted MRI scans of C26 colon carcinoma xenograft model; administered through tail vein	180
Rhodamine B encapsulated PLGA nanoparticles	50 : 50; Rhodamine B	Dewetting technique	80; 93.26%	Human A549lung cancer cells for fluorescence imaging	181
AS1411 aptamer conjugated curcumin and SPIONs encapsulated PLGA nanocapsule	Curcumin and superparamagnetic iron oxide nanoparticles (SPIONs)	Nanoprecipitation	150; —	Pancreatic cancer cells (PANC-1 and MIA PaCa-2) for optical, MRI, and photoacoustic imaging	182
CN-PPV and NIR dye encapsulate PLGA nanoparticle	50 : 50; Red-emitting conjugated polymer (CN-PPV) and near-infrared dye (NIR)	Single-emulsion solvent evaporation	50; —	Cervical cancer cells (HeLa) for optical imaging	183
Doxorubicin encapsulated and Cy5.5 labeled PLGA nanoparticle	50 : 50; Doxorubicin, Cy5.5	Double emulsion solvent evaporation	114; ∼80%	U87 human glioma cell line for optical imaging and drug delivery	184
Polyethyleneimine-polyethylene glycol-folic acid functionalized quantum dots, Fe$_3$O$_4$ nanocrystals, and doxorubicin (DOX) encapsulated and (shRNA) adsorbed PLGA nanocomposites	50 : 50; CdSe/ZnS quantum dots, superparamagnetic Fe$_3$O$_4$ nanocrystals, Doxorubicin (DOX) and vascular endothelial growth factor (VEGF)-targeted small hairpin RNA (shRNA)	Double emulsion solvent evaporation	∼300 nm; ∼62.97% for DOX	Cervical cancer cells (HeLa) and subcutaneous EMT-6 tumor xenograft mice model for MR and fluorescence imaging and drug delivery; Administered through intratumoral injection	185
Curcumin encapsulated PLGA nanoparticle	50 : 50; Curcumin	Microfluidic	30–70; 67%	Leukemia Jurkat cells for drug delivery	186
Chitosan and PEG-coated curcumin-loaded PLGA nanoparticles (CNPs)	50 : 50; Curcumin	Single-emulsion solvent evaporation	264 nm; 60%	Human pancreatic cancer cell lines PANC-1 and Mia Paca-2 for drug delivery	187
OX26 type monoclonal antibody functionalized TMZ encapsulated PLGA nanoparticle	50 : 50; Temozolomide (TMZ)	Single-emulsion solvent evaporation	176; 48 ± 10%	Glioblastoma cells (U215 and U87) for drug delivery	188
DOX encapsulated and Au nanoparticle decorated PLGA nanoparticle	50 : 50; Doxorubicin (DOX)	Double emulsion solvent evaporation	∼160; —	Mouse colon cancer cells (CT26), Murine breast cancer cells (4T1) and mice bearing 4T1 tumors for photoacoustic imaging and drug delivery; administered through intravenous mode	189
Transferrin decorated paclitaxel and elacridar co-encapsulated PLGA nanoparticle	Transferrin and elacridar	Nanoprecipitation	226.9; 76%	Drug-resistant breast cancer cells (EMT6/AR1.0) for drug delivery	190
MTX and CUR co-encapsulated PLGA nanoparticle	Methotrexate (MTX) and curcumin (CUR)	Double emulsion solvent evaporation	142.3 ± 4.07; MTX 71.32 ± 7.8% and CUR 85.64 ± 6.3%	Breast cancer cells SK-Br-3 cell line and chemically induced mammary tumors in female Sprague Dawley rats for drug delivery; administered through intravenous mode	191
iRGD conjugated and PTX-loaded PLGA nanoparticle	Paclitaxel (PTX)	Single-emulsion solvent evaporation	147.5 ± 9.5; 88.2%	Human colorectal cancer cells (LS174T, COLO205, HCT116, and SW620) and LS174T tumor-bearing BALB/c (nu/nu) mice for drug delivery; Administered through intravenous mode	192

Table 4 (continued)

Nanoparticle formulation	LA : GA and Type of imaging/ drug molecules	Synthesis method	Size (nm) and encapsulation efficiency	Application on and administration route	Ref.
Curcumin and Niclosamide encapsulated PLGA nanoparticle	50 : 50; Curcumin and niclosamide	Nanoprecipitation	225.9; 58.09% for Curcumin and 85.36% for Niclosamide	Breast cancer cells (MDA-MB-231) for drug delivery	193
Epidermal growth factor functionalized 5Fu and perfluorocarbon (PFC) co-loaded PLGA nanoparticle	5-Fluorouracil (5Fu)	Double emulsion solvent evaporation	200; 81.6 ± 5.7%	Human colon cancer cells (SW620) for drug delivery	194
Cannabidiol (CBD) loaded PLGA nanoparticle	Cannabidiol (CBD)	Single-emulsion solvent evaporation	240; 95%	Epithelial ovarian cancer cells (SKOV-3) for drug delivery	195
Sal and Tam encapsulated (PEG)–PLGA nanoparticle	75 : 25; Salidroside (Sal) and Tamoxifen (Tam)	Double emulsion solvent evaporation	275.3 ± 44.0; Sal 32.63% ± 0.73% and Tam 49.18% ± 3.04%	Mouse breast cancer cell line (4T1) and female BALB/c mice for drug delivery; administered through intraperitoneal mode	196
Tg conjugated PLGA nanoparticle	50 : 50; 6-Thioguanine (Tg)	Electrospray	∼60 nm; 97.22%	Cervical cancer cells (HeLa) for drug delivery and fluorescence imaging	90
PBA conjugated and MTX decorated PLGA nanoparticle	50 : 50; 1-pyrenebutyric acid (PBA) and methotrexate (MTX)	Electrospray	∼105 nm 91.4%	MTX resistant metastatic breast cancer cells (MCF-7 and MDA-MB-231) for fluorescence imaging and drug delivery	91
Molybdenum octahedral clusters encapsulated PLGA nanoparticle	50 : 50; Molybdenum octahedral clusters	Single-emulsion solvent evaporation	75.7–144.7; 29.2–73.9%	Ovarian cancer cell line (A2780) for photodynamic therapy (PDT)	197
PNAs encapsulated PLGA nanoparticle	Short cationic peptide nucleic acids (PNAs)	Double emulsion solvent evaporation	145; —	HeLa, A549, HEK-293, SUDHL-5, U2932 cell line and xenograft mouse model for drug delivery; administered through tail vein	198

diglycol L-glutamate) (VEOEG) that can inhibit drug efflux and with prolonged blood circulation time in an *in vivo* system. VEOEG surfactant coated and paclitaxel (PTX) loaded PLGA nanoparticle was conjugated with hyaluronic acid (PTX-HA-PLGA NPs), specifically targeting CD44 receptor overexpressed on various cancer cells. These PTX-HA-PLGA NPs exhibited excellent stability without any burst release of PTX with increased plasma half-life in *in vivo*.[160] To achieve the most critical aspects of the therapeutic delivery vehicle, such as colloidal stability, high therapeutic payload, and controlled drug release at the target site, Wang *et al.* synthesized doxorubicin (DOX) encapsulated bio-responsive multifunctional PLGA nanoparticles from reversible crosslinking of lipoic acid modified star PLGA polymer. Specific release of doxorubicin from those nanoparticles in the intracellular reductive environment of cancer cells improved accumulation inside the tumor and reduced systemic side effects, which significantly enhanced cancer chemotherapeutic efficacy.[161]

The research works carried out in the last decade on PLGA nano-carriers and their applications in cancer therapy are discussed in Table 4.

6 Current limitations and future perspectives

After surveying the literature, it is found that there are some limitations in the reported PLGA nanoparticle synthesis. Most of the methods employ more than one solvent phase with stabilizer/cross-linker and high shear stress for a prolonged time, resulting in drug loss, agglomeration, and polydispersity in the nanoparticle size. Nevertheless, some residual solvents may remain after several washes, imparting undesirable toxic effects during the application phase. Moreover, during drug delivery, it is necessary to track the traveling pathway of nanoparticles. Therefore, stable imaging property with high intensity imaging is essential for monitoring the drug delivery vehicle after it is administered. Incorporating therapeutic and imaging molecules in a single nano-platform requires an environment in which both of them would not lose their molecular properties by interacting with each other. Thus, there are considerable challenges to encapsulate both molecules in a single particle such as (a) ionic property and hydrophobicity of both molecules may precipitate out one of them in a single solvent phase, (b) encapsulation efficiency of the drug may reduce, (c) imaging molecules may also release from the nanoparticles, which would result in misleading of the tracking of nanoparticles. To overcome these limitations, a fabrication process is required, which should be facile, efficient, and tuneable for achieving different integral properties like narrow size distribution, sustained-release kinetics, and capability to deliver different imaging/drug molecules by a single carrier. This requires developing an automated PLGA fabrication setup to synthesize nanoparticles with different molecules in a pre-programmed way that could save time and effort for large-scale synthesis.

There is a vast research scope to continue this exploration with modern drug molecules that can be conveyed using PLGA nano-carriers and unveil their applications beyond the cellular model. Their behavior may be studied in *in vitro* 3D tumor spheroid, which mimics the complex *in vivo* tumor vasculature

on a benchtop. It would be beneficial for the real-time study of drug delivery and imaging efficacy of nano-carriers. This type of study may also provide information regarding tumor vasculature penetration capability, size reducing efficiency of the tumor, cytotoxic efficiency, and monitoring ability of the therapeutic responses. Finally, the nano-carrier efficiency may be studied in clinical trials to understand better the effectiveness as a theranostic nano-system in cancer management.

7 Conclusion

The nanoparticle is becoming a promising alternative to conventional chemotherapeutic drugs as they cover-up all the limitations that reduce the success rate of the chemotherapeutic treatment. Nevertheless, it also appears to be an excellent tool for monitoring the diseased area and treatment responses. For this purpose, polymeric nanoparticles have gained huge interest due to their flexibility in synthesis, chemical modification, and drug release kinetics. The majority of the polymeric nanoparticles are fabricated using numerous biocompatible polymers to reduce the undesirable systemic toxicity of the drug transporter. Among various polymers, FDA and EMA approved biodegradable PLGA polymer is the most widely used as a versatile and clinically proven polymer for the synthesis of efficient nano-carrier for biomedical applications. An equal ratio of lactic acid and glycolic acid containing PLGA chain with low molecular weight is predominantly used to synthesize the nano-carrier system as it manifests optimum hydrolysis rate compared to other monomeric ratio compositions in PLGA chains. PLGA nano-carrier can be synthesized through a wide range of techniques. It has better stability, allows easy modification, and provides control over the drug release rate. The existing nanoparticle synthesis techniques face some challenges and that might compromise the therapeutic efficiency of the nano-carrier. Among all the techniques, the electrospray method is comparatively newer, convenient, and effective against most of the existing limitations. For active delivery of drug/imaging molecules, functionalization steps are used for covalent and noncovalent modifications of the polymer before or after synthesis of the nanoparticle. There is some lack of long term stability and constant intensity of the monitoring agents as they are simply encapsulated inside the particles. For stable monitoring, the inherent imaging quality of theranostic nanoparticles is necessary to study the real time effect of the delivery agents.

Conflicts of interest

There are no conflicts to declare.

Acknowledgements

References

1 R. Krukemeyer, M. G. Krenn, V. Huebner, F. Wagner and W. Resch, *J. Nanomed. Nanotechnol.*, 2015, **6**(6), 336.

2 S. Bayda, M. Adeel, T. Tuccinardi, M. Cordani and F. Rizzolio, *Molecules*, 2020, **25**, 1–15.

3 A. P. Ramos, M. A. E. Cruz, C. B. Tovani and P. Ciancaglini, *Biophys. Rev.*, 2017, **9**, 79–89.

4 H. A. Khan, M. K. Sakharkar, A. Nayak, U. Kishore and A. Khan, *Nanoparticles for biomedical applications: An overview*, Elsevier Ltd., 2018.

5 R. Shukla, N. Chanda, A. Zambre, A. Upendran, K. Katti, R. R. Kulkarni, S. K. Nune, S. W. Casteel, C. J. Smith, J. Vimal, E. Boote, J. D. Robertson, P. Kan, H. Engelbrecht, L. D. Watkinson, T. L. Carmack, J. R. Lever, C. S. Cutler, C. Caldwell, R. Kannan and K. V. Katti, *Proc. Natl. Acad. Sci. U. S. A.*, 2012, **109**, 12426–12431.

6 P. Christian, F. Von Der Kammer, M. Baalousha and T. Hofmann, *Ecotoxicology*, 2008, **17**, 326–343.

7 M. A. Gatoo, S. Naseem, M. Y. Arfat, A. Mahmood Dar, K. Qasim and S. Zubair, *Biomed Res. Int.*, 2014, 498420.

8 P. Kumbhakar, S. S. Ray and A. L. Stepanov, *J. Nanomater.*, 2014, **2014**, 2–4.

9 H. Zhu, E. Prince, P. Narayanan, K. Liu, Z. Nie and E. Kumacheva, *Chem. Commun.*, 2020, **56**, 8131–8134.

10 D. Suresh, A. Zambre, N. Chanda, T. J. Hoffman, C. J. Smith, J. D. Robertson and R. Kannan, *Bioconjugate Chem.*, 2014, **25**, 1565–1579.

11 L. Zhang, F. X. Gu, J. M. Chan, A. Z. Wang, R. S. Langer and O. C. Farokhzad, *Clin. Pharmacol. Ther.*, 2008, **83**, 761–769.

12 R. Wang, P. S. Billone and W. M. Mullett, *J. Coast. Life Med.*, 2013, 629681.

13 V. Weissig, T. K. Pettinger and N. Murdock, *Int. J. Nanomed.*, 2014, **9**, 4357–4373.

14 Y. H. Choi and H. K. Han, *J. Pharm. Invest.*, 2018, **48**, 43–60.

15 C. L. Ventola, *Pharmacol. Ther.*, 2017, **42**, 742–755.

16 A. Zambre, N. Chanda, S. Prayaga, R. Almudhafar, Z. Afrasiabi, A. Upendran and R. Kannan, *Anal. Chem.*, 2012, **84**, 9478–9484.

17 B. Blasiak, F. C. J. M. Van Veggel and B. Tomanek, *J. Nanomater.*, 2013, 148578.

18 H. Bin Na, I. C. Song and T. Hyeon, *Adv. Mater.*, 2009, **21**, 2133–2148.

19 Y. Liu, K. Ai, J. Liu, Q. Yuan, Y. He and L. Lu, *Adv. Healthcare Mater.*, 2012, **1**, 461–466.

20 E. Kang, H. S. Min, J. Lee, M. H. Han, H. J. Ahn, I. C. Yoon, K. Choi, K. Kim, K. Park and I. C. Kwon, *Angew. Chem., Int. Ed.*, 2010, **49**, 524–528.

21 X. Cai, W. Li, C. Kim, Y. Yuan, L. V. Wang and Y. Xia, *ACS Nano*, 2011, **5**, 9658–9667.

22 H. Xie, Z. J. Wang, A. Bao, B. Goins and W. T. Phillips, *Int. J. Pharm.*, 2010, **395**, 324–330.

23 K. Kim, J. H. Kim, H. Park, Y. S. Kim, K. Park, H. Nam, S. Lee, J. H. Park, R. W. Park, I. S. Kim, K. Choi, S. Y. Kim, K. Park and I. C. Kwon, *J. Controlled Release*, 2010, **146**, 219–227.

24 N. Chanda, A. Upendran, E. J. Boote, A. Zambre, S. Axiak, K. Selting, K. V. Katti, W. M. Leevy, Z. Afrasiabi, J. Vimal, J. Singh, J. C. Lattimer and R. Kannan, *J. Biomed. Nanotechnol.*, 2014, **10**, 383–392.

25 C. A. Wathen, C. Caldwell, N. Chanda, A. Upendran, A. Zambre, Z. Afrasiabi, S. E. Chapaman, N. Foje, W. M. Leevy and R. Kannan, *Contrast Media Mol. Imaging*, 2015, **10**, 188–193.

26 Y. F. Li and C. Chen, *Small*, 2011, **7**, 2965–2980.

27 X. D. Zhang, H. Y. Wu, D. Wu, Y. Y. Wang, J. H. Chang, Z. Bin Zhai, A. M. Meng, P. X. Liu, L. A. Zhang and F. Y. Fan, *Int. J. Nanomed.*, 2010, **5**, 771–781.

28 N. Larson and H. Ghandehari, *Chem. Mater.*, 2012, **24**, 840–853.

29 H. Maeda, T. Sawa and T. Konno, *J. Controlled Release*, 2001, **74**, 47–61.

30 G. Pasut and F. M. Veronese, *Prog. Polym. Sci.*, 2007, **32**, 933–961.

31 Y. Shen, E. Jin, B. Zhang, C. J. Murphy, M. Sui, J. Zhao, J. Wang, J. Tang, M. Fan, E. Van Kirk and W. J. Murdoch, *J. Am. Chem. Soc.*, 2010, **132**, 4259–4265.

32 L. Dai, R. Liu, L. Q. Hu, Z. F. Zou and C. L. Si, *ACS Sustainable Chem. Eng.*, 2017, **5**, 8241–8249.

33 E. Calzoni, A. Cesaretti, A. Polchi, A. Di Michele, B. Tancini and C. Emiliani, *J. Funct. Biomater.*, 2019, **10**, 1–15.

34 M. Hirenkumar and S. Steven, *Polymers*, 2012, **3**, 1–19.

35 P. Gentile, V. Chiono, I. Carmagnola and P. V. Hatton, *Int. J. Mol. Sci.*, 2014, **15**, 3640–3659.

36 F. Danhier, E. Ansorena, J. M. Silva, R. Coco, A. Le Breton and V. Préat, *J. Controlled Release*, 2012, **161**, 505–522.

37 E. M. M. L. Houchin, TOPP, *J. Pharm. Sci.*, 2007, **97**, 2395–2404.

38 A. Kumari, S. K. Yadav and S. C. Yadav, *Colloids Surf., B*, 2010, **75**, 1–18.

39 E. Swider, O. Koshkina, J. Tel, L. J. Cruz, I. J. M. de Vries and M. Srinivas, *Acta Biomater.*, 2018, **73**, 38–51.

40 S. Rezvantalab, N. I. Drude, M. K. Moraveji, N. Güvener, E. K. Koons, Y. Shi, T. Lammers and F. Kiessling, *Front. Pharmacol.*, 2018, **9**, 1–19.

41 M. Ayyoob and Y. J. Kim, *Polymers*, 2018, **10**, 1–16.

42 T. D. Farahani, A. A. Entezami, H. Mobedi and M. Abtahi, *Iran. Polym. J.*, 2005, **14**, 753–763.

43 D. D. Von Hoff, M. M. Mita, R. K. Ramanathan, G. J. Weiss, A. C. Mita, P. M. Lorusso, H. A. Burris, L. L. Hart, S. C. Low, D. M. Parsons, S. E. Zale, J. M. Summa, H. Youssoufian and J. C. Sachdev, *Clin. Cancer Res.*, 2016, **22**, 3157–3163.

44 A. C. Anselmo and S. Mitragotri, *Bioeng. Transl. Med.*, 2016, **1**, 10–29.

45 H. Zhong, G. Chan, Y. Hu, H. Hu and D. Ouyang, *Pharmaceutics*, 2018, **10**, 1–19.

46 K. Park, S. Skidmore, J. Hadar, J. Garner, H. Park, A. Otte, B. K. Soh, G. Yoon, D. Yu, Y. Yun, B. K. Lee, X. Jiang and Y. Wang, *J. Controlled Release*, 2019, **304**, 125–134.

47 Y. Dang and J. Guan, *Smart Mater. Med.*, 2020, **1**, 10–19.

48 J. Hadar, S. Skidmore, J. Garner, H. Park, K. Park, Y. Wang, B. Qin and X. Jiang, *J. Controlled Release*, 2019, **304**, 75–89.

49 ELIGARD®, https://www.accessdata.fda.gov/drugsatfda_docs/label/2007/021731s005,021488s010,021379s010,021343s015lbl.pdf.

50 SIGNIFOR LAR®, https://www.accessdata.fda.gov/drugsatfda_docs/label/2020/203255s008lbl.pdf.

51 J. Zhou, J. Walker, R. Ackermann, K. Olsen, J. K. Y. Hong, Y. Wang and S. P. Schwendeman, *Mol. Pharm.*, 2020, **17**, 1502–1515.

52 S. Pieper and K. Langer, *Mater. Today Proc.*, 2017, **4**, S188–S192.

53 H. Y. Kwon, J. Y. Lee, S. W. Choi, Y. Jang and J. H. Kim, *Colloids Surf., A*, 2001, **182**, 123–130.

54 C. E. Astete, C. S. S. R. Kumar and C. M. Sabliov, *Colloids Surf., A*, 2007, **299**, 209–216.

55 D. Cun, D. K. Jensen, M. J. Maltesen, M. Bunker, P. Whiteside, D. Scurr, C. Foged and H. M. Nielsen, *Eur. J. Pharm. Biopharm.*, 2011, **77**, 26–35.

56 K. Kizilbey, *ACS Omega*, 2019, **4**, 555–562.

57 M. J. Ramalho and M. C. Pereira, *J. Chem. Educ.*, 2016, **93**, 1446–1451.

58 K. Y. Hernández-Giottonini, R. J. Rodríguez-Córdova, C. A. Gutiérrez-Valenzuela, O. Peñuñuri-Miranda, P. Zavala-Rivera, P. Guerrero-Germán and A. Lucero-Acuña, *RSC Adv.*, 2020, **10**, 4218–4231.

59 Y. Javadzadeh, F. Ahadi, S. Davaran, G. Mohammadi, A. Sabzevari and K. Adibkia, *Colloids Surf., B*, 2010, **81**, 498–502.

60 R. Manchanda, A. Fernandez-Fernandez, A. Nagesetti and A. J. McGoron, *Colloids Surf., B*, 2010, **75**, 260–267.

61 J. M. Barichello, M. Morishita, K. Takayama, T. Nagai, J. M. Barichello and M. Morishita, *Drug Dev. Ind. Pharm.*, 1999, **25**, 471–476.

62 G. Wang, B. Yu, Y. Wu, B. Huang, Y. Yuan and C. S. Liu, *Int. J. Pharm.*, 2013, **446**, 24–33.

63 W. S. Saad and R. K. Prud'Homme, *Nano Today*, 2016, **11**, 212–227.

64 F. Lince, D. L. Marchisio and A. A. Barresi, *J. Colloid Interface Sci.*, 2008, **322**, 505–515.

65 C. G. Barreras-Urbina, B. Ramírez-Wong, G. A. López-Ahumada, S. E. Burruel-Ibarra, O. Martínez-Cruz, J. A. Tapia-Hernández and F. Rodríguez Félix, *Int. J. Food Prop.*, 2016, **19**, 1912–1923.

66 M. S. Muthu, M. K. Rawat, A. Mishra and S. Singh, *Nanomedicine*, 2009, **5**, 323–333.

67 C. Arpagaus, *J. Pharm. Invest.*, 2019, **49**, 405–426.

68 Y. Kohl, C. Kaiser, W. Bost, F. Stracke, M. Fournelle, C. Wischke, H. Thielecke, A. Lendlein, K. Kratz and R. Lemor, *Nanomedicine*, 2011, **7**, 228–237.

69 D. M. K. Jensen, D. Cun, M. J. Maltesen, S. Frokjaer, H. M. Nielsen and C. Foged, *J. Controlled Release*, 2010, **142**, 138–145.

70 A. Panda, J. Meena, R. Katara and D. K. Majumdar, *Pharm. Dev. Technol.*, 2016, **21**, 43–53.

71 X. Li, N. Anton, C. Arpagaus, F. Belleteix and T. F. Vandamme, *J. Controlled Release*, 2010, **147**, 304–310.

72 A. Sosnik and K. P. Seremeta, *Adv. Colloid Interface Sci.*, 2015, **223**, 40–54.

73 N. Mendoza-Munoz, D. Quintanar-Guerrero and E. Allemann, *Recent Pat. Drug Delivery Formulation*, 2012, **6**, 236–249.

74 Y. N. Konan, R. Gurny and E. Allemann, *Int. J. Pharm.*, 2002, **233**, 239–252.

75 X. Song, Y. Zhao, W. Wu, Y. Bi, Z. Cai, Q. Chen, Y. Li and S. Hou, *Int. J. Pharm.*, 2008, **350**, 320–329.

76 M. L. T. Zweers, D. W. Grijpma, G. H. M. Engbers and J. Feijen, *J. Biomed. Mater. Res., Part B*, 2003, **66**, 559–566.

77 S. Rezvantalab and M. Keshavarz Moraveji, *RSC Adv.*, 2019, **9**, 2055–2072.

78 L. L. Li, X. Li and H. Wang, *Small Methods*, 2017, **1**, 1–9.

79 J. Wang, W. Chen, J. Sun, C. Liu, Q. Yin, L. Zhang, Y. Xianyu, X. Shi, G. Hu and X. Jiang, *Lab Chip*, 2014, **14**, 1673–1677.

80 Z. Mahmoodi, J. Mohammadnejad, S. Razavi Bazaz, A. Abouei Mehrizi, M. A. Ghiass, M. Saidijam, R. Dinarvand, M. Ebrahimi Warkiani and M. Soleimani, *Drug Delivery Transl. Res.*, 2019, **9**, 707–720.

81 J. P. Rolland, B. W. Maynor, L. E. Euliss, A. E. Exner, G. M. Denison, J. M. Desimone, C. Hill, N. Carolina and C. Engineering, *J. Am. Chem. Soc.*, 2005, **127**, 10096–10100.

82 E. M. Enlow, J. C. Luft, M. E. Napier and J. M. Desimone, *Nano Lett.*, 2011, **11**, 808–813.

83 B. L. Banik, P. Fattahi and J. L. Brown, *Wiley Interdiscip. Rev.: Nanomed. Nanobiotechnol.*, 2016, **8**, 271–299.

84 D. Essa, P. P. D. Kondiah, Y. E. Choonara and V. Pillay, *Front. Bioeng. Biotechnol.*, 2020, **8**, 1–20.

85 W. Hasan, K. Chu, A. Gullapalli, S. S. Dunn, M. Elizabeth, Φ. Enlow, J. C. Luft, S. Tian, M. E. Napier, P. D. Pohlhaus, J. P. Rolland, J. M. Desimone, U. States and N. York, *Nano Lett.*, 2012, **12**, 287–292.

86 K. S. Chu, W. Hasan, S. Rawal, M. D. Walsh, E. M. Enlow, J. C. Luft, A. S. Bridges, J. L. Kuijer, M. E. Napier, W. C. Zamboni and J. M. DeSimone, *Nanomedicine*, 2013, **9**, 686–693.

87 J. A. Tapia-Hernández, P. I. Torres-Chávez, B. Ramírez-Wong, A. Rascón-Chu, M. Plascencia-Jatomea, C. G. Barreras-Urbina, N. A. Rangel-Vázquez and F. Rodríguez-Félix, *J. Agric. Food Chem.*, 2015, **63**, 4699–4707.

88 D. N. Nguyen, C. Clasen and G. Van den Mooter, *J. Pharm. Sci.*, 2016, **105**, 2601–2620.

89 B. Almería, W. Deng, T. M. Fahmy and A. Gomez, *J. Colloid Interface Sci.*, 2010, **343**, 125–133.

90 M. Chatterjee, N. Jaiswal, A. Hens, N. Mahata and N. Chanda, *Mater. Sci. Eng., C*, 2020, **114**, 111029.

91 M. Chatterjee, R. Maity, S. Das, N. Mahata, B. Basu and N. Chanda, *Mater. Adv.*, 2020, **1**, 3033–3048.

92 A. Juan, F. J. Cimas, I. Bravo, A. Pandiella, A. Ocaña and C. Alonso-Moreno, *Pharmaceutics*, 2020, **12**, 1–20.

93 J. Nicolas, S. Mura, D. Brambilla, N. Mackiewicz and P. Couvreur, *Chem. Soc. Rev.*, 2013, **42**, 1147–1235.

94 W. X. Ren, J. Han, S. Uhm, Y. J. Jang, C. Kang, J. H. Kim and J. S. Kim, *Chem. Commun.*, 2015, **51**, 10403–10418.

95 C. Akshay and J. Kun, *J. Controlled Release*, 2017, **245**, 27–40.

96 R. W. Sirianni, M. Q. Zheng, T. R. Patel, T. Shafbauer, J. Zhou, W. M. Saltzman, R. E. Carson and Y. Huang, *Bioconjugate Chem.*, 2014, **25**, 2157–2165.

97 N. Nakajima and Y. Ikada, *Bioconjugate Chem.*, 1995, **6**, 123–130.

98 Q. Yan, H. N. Zheng, C. Jiang, K. Li and S. J. Xiao, *RSC Adv.*, 2015, **5**, 69939–69947.

99 J. V. Staros, R. W. Wright and D. M. Swingle, *Anal. Biochem.*, 1986, **156**, 220–222.

100 D. F. Detar and R. Silverstein, *J. Am. Chem. Soc.*, 1966, **88**, 1013–1019.

101 H. Shen, A. M. Jawaid and P. T. Snee, *ACS Nano*, 2009, **3**, 915–923.

102 N. Jaiswal, A. Hens, M. Chatterjee, N. Mahata and N. Chanda, *J. Colloid Interface Sci.*, 2019, **534**, 122–130.

103 N. Zhang, C. Chittasupho, C. Duangrat, T. J. Siahaan and C. Berkland, *Bioconjugate Chem.*, 2008, **19**, 145–152.

104 N. Graf, D. R. Bielenberg, N. Kolishetti, C. Muus, J. Banyard, O. C. Farokhzad and S. J. Lippard, *ACS Nano*, 2012, **6**, 4530–4539.

105 Y. Liu, K. Li, B. Liu and S. S. Feng, *Biomaterials*, 2010, **31**, 9145–9155.

106 B. H. Northrop, S. H. Frayne and U. Choudhary, *Polym. Chem.*, 2015, **6**, 3415–3430.

107 K. Renault, J. W. Fredy, P. Y. Renard and C. Sabot, *Bioconjugate Chem.*, 2018, **29**, 2497–2513.

108 L. Martínez-Jothar, S. Doulkeridou, R. M. Schiffelers, J. Sastre Torano, S. Oliveira, C. F. van Nostrum and W. E. Hennink, *J. Controlled Release*, 2018, **282**, 101–109.

109 Sulfhydryl-reactive Crosslinker Chemistry, https://www.thermofisher.com/in/en/home/life-science/protein-biology/protein-biology-learning-center/protein-biology-resource-library/pierce-protein-methods/sulfhydryl-reactive-crosslinker-chemistry.html.

110 J. Su, *Gels*, 2018, **4**, 72.

111 A. Vasconcelos, E. Vega, Y. Pérez, M. J. Gómara, M. L. García and I. Haro, *Int. J. Nanomed.*, 2015, **10**, 609–631.

112 P. Akkapeddi, S. A. Azizi, A. M. Freedy, P. M. S. D. Cal, P. M. P. Gois and G. J. L. Bernardes, *Chem. Sci.*, 2016, **7**, 2954–2963.

113 G. D. Paka and C. Ramassamy, *Mol. Pharm.*, 2017, **14**, 93–106.

114 P. J. Kennedy, F. Sousa, D. Ferreira, C. Pereira, M. Nestor, C. Oliveira, P. L. Granja and B. Sarmento, *Acta Biomater.*, 2018, **81**, 208–218.

115 C. W. Tornøe, C. Christensen and M. Meldal, *J. Org. Chem.*, 2002, **67**, 3057–3064.

116 V. V. Rostovtsev, L. G. Green, V. V. Fokin and K. B. Sharpless, *Angew. Chem., Int. Ed.*, 2002, **41**, 2596–2599.

117 V. Hong, S. I. Presolski, C. Ma and M. G. Finn, *Angew. Chem., Int. Ed.*, 2009, **48**, 9879–9883.

118 J. Lu, M. Shi and M. S. Shoichet, *Bioconjugate Chem.*, 2009, **20**, 87–94.

119 E. Haldón, M. C. Nicasio and P. J. Pérez, *Org. Biomol. Chem.*, 2015, **13**, 9528–9550.

120 C. Spiteri and J. E. Moses, *Angew. Chem., Int. Ed.*, 2010, **49**, 31–33.

121 F. Himo, T. Lovell, R. Hilgraf, V. V. Rostovtsev, L. Noodleman, K. B. Sharpless and V. V. Fokin, *J. Am. Chem. Soc.*, 2005, **127**, 210–216.

122 A. O. Saeed, J. P. Magnusson, E. Moradi, M. Soliman, W. Wang, S. Stolnik, K. J. Thurecht, S. M. Howdle and C. Alexander, *Bioconjugate Chem.*, 2011, **22**, 156–168.

123 Z. Zhou, A. Badkas, M. Stevenson, J. Y. Lee and Y. K. Leung, *Int. J. Pharm.*, 2015, **487**, 81–90.

124 C. Fonseca, S. Simões and R. Gaspar, *J. Controlled Release*, 2002, **83**, 273–286.

125 C. E. Astete and C. M. Sabliov, *J. Biomater. Sci., Polym. Ed.*, 2006, **17**, 247–289.

126 W. Huang and C. Zhang, *Biotechnol. J.*, 2018, **13**, 1–19.

127 B. Zhang, P. Sai Lung, S. Zhao, Z. Chu, W. Chrzanowski and Q. Li, *Sci. Rep.*, 2017, **7**, 1–8.

128 M. Chatterjee, A. Hens, K. Mahato, N. Jaiswal, N. Mahato, Nagahanumaiah and N. Chanda, *J. Colloid Interface Sci.*, 2017, **506**, 126–134.

129 D. H. Jo, J. H. Kim, T. G. Lee and J. H. Kim, *Nanomedicine*, 2015, **11**, 1603–1611.

130 N. Ma, C. Ma, C. Li, T. Wang, Y. Tang, H. Wang, X. Mou, Z. Chen and N. He, *J. Nanosci. Nanotechnol.*, 2013, **13**, 6485–6498.

131 S. Prabha, G. Arya, R. Chandra, B. Ahmed and S. Nimesh, *Artif. Cells, Nanomed., Biotechnol.*, 2016, **44**, 83–91.

132 S. Honary and F. Zahir, *Trop. J. Pharm. Res.*, 2013, **12**, 265–273.

133 J. Sitterberg, A. Özcetin, C. Ehrhardt and U. Bakowsky, *Eur. J. Pharm. Biopharm.*, 2010, **74**, 2–13.

134 R. Carvalho Silva, L. Alexandre Muehlmann, J. Rodrigues Da Silva, R. de Bentes Azevedo and C. Madeira Lucci, *Microsc. Res. Tech.*, 2014, **77**, 691–696.

135 S. Spek, M. Haeuser, M. M. Schaefer and K. Langer, *Appl. Surf. Sci.*, 2015, **347**, 378–385.

136 A. Romani, C. Clementi, C. Miliani and G. Favaro, *Acc. Chem. Res.*, 2010, **43**, 837–846.

137 H. Freichels, F. Danhier, V. Préat, P. Lecomte and C. Jérôme, *Int. J. Artif. Organs*, 2011, **34**, 152–160.

138 L. M. do, A. C. Gaspar, A. C. S. Dórea, D. Droppa-Almeida, I. S. de Mélo Silva, F. E. Montoro, L. L. Alves, M. L. H. Macedo and F. F. Padilha, *J. Nanoparticle Res.*, 2018, **20**, 289.

139 S. F. Peng, C. Y. Lee, M. J. Hour, S. C. Tsai, D. H. Kuo, F. A. Chen, P. C. Shieh and J. S. Yang, *Int. J. Oncol.*, 2014, **44**, 238–246.

140 C. S. S. R. Kumar, *Raman spectroscopy for nanomaterials characterization*, 2012, vol. 9783642206.

141 Cancer, https://www.who.int/news-room/fact-sheets/detail/cancer.

142 No Title, https://www.iarc.fr/featured-news/latest-global-cancer-data-cancer-burden-rises-to-19-3-million-new-cases-and-10-0-million-cancer-deaths-in-2020/.

143 Global Cancer Data: GLOBOCAN 2018, https://www.uicc.org/news/new-global-cancer-data-globocan-2018.

144 GLOBOCAN 2020: New Global Cancer Data, https://www.uicc.org/news/globocan-2020-new-cancer-data#.

145 V. Hanf and R. Kreienberg, *WHO report on cancer: setting priorities, investing wisely and providing care for all*, 2003.

146 M. Arruebo, N. Vilaboa, B. Sáez-Gutierrez, J. Lambea, A. Tres, M. Valladares and Á. González-Fernández, *Cancers*, 2011, **3**, 3279–3330.

147 L. Salvioni, M. A. Rizzuto, J. A. Bertolini, L. Pandolfi, M. Colombo and D. Prosperi, *Cancers*, 2019, **11**(12), 1855.

148 G. Bor, I. D. M. Azmi and A. Yaghmur, *Ther. Delivery*, 2019, **10**, 113–132.

149 K. H. Bae, H. J. Chung and T. G. Park, *Mol. Cells*, 2011, **31**, 295–302.

150 X. Wang, L. Yang, Z. Chen and D. M. Shin, *CA-Cancer J. Clin.*, 2008, **58**, 97–110.

151 L. Smith, Z. Kuncic, K. Ostrikov and S. Kumar, *J. Nanomater.*, 2012, **2012**, 891318.

152 S. Chapman, M. Dobrovolskaia, K. Farahani, A. Goodwin, A. Joshi, H. Lee, T. Meade, M. Pomper, K. Ptak, J. Rao, R. Singh, S. Sridhar, S. Stern, A. Wang, J. B. Weaver, G. Woloschak and L. Yang, *Nano Today*, 2013, **8**, 454–460.

153 J. Zugazagoitia, C. Guedes, S. Ponce, I. Ferrer, S. Molina-Pinelo and L. Paz-Ares, *Clin. Ther.*, 2016, **38**, 1551–1566.

154 J. S. Xu, J. Huang, R. Qin, G. H. Hinkle, S. P. Povoski, E. W. Martin and R. X. Xu, *Biomaterials*, 2010, **31**, 1716–1722.

155 A. J. Mieszawska, A. Gianella, D. P. Cormode, Y. Zhao, A. Meijerink, R. Langer, O. C. Farokhzad, Z. A. Fayad and W. J. M. Mulder, *Chem. Commun.*, 2012, **48**, 5835–5837.

156 R. N. Mariano, D. Alberti, J. C. Cutrin, S. G. Crich and S. Aime, *Mol. Pharm.*, 2014, **11**, 4100–4106.

157 X. Wang, L. Yang, H. Zhang, B. Tian, R. Li, X. Hou and F. Wei, *Colloids Surf., B*, 2018, **172**, 708–717.

158 Z. Amoozgar, J. Park, Q. Lin and Y. Yeo, *Mol. Pharm.*, 2012, **9**, 1262–1270.

159 R. Devulapally, K. Foygel, T. V. Sekar, J. K. Willmann and R. Paulmurugan, *ACS Appl. Mater. Interfaces*, 2016, **8**, 33412–33422.

160 J. Wu, J. Zhang, C. Deng, F. Meng and Z. Zhong, *Biomacromolecules*, 2016, **17**, 2367–2374.

161 X. Wang, R. Cheng, L. Cheng and Z. Zhong, *Biomacromolecules*, 2018, **19**, 1368–1373.

162 J. Kim, J. E. Lee, S. H. Lee, J. H. Yu, J. H. Lee, T. G. Park and T. Hyeon, *Adv. Mater.*, 2008, **20**, 478–483.

163 X. R. Song, Z. Cai, Y. Zheng, G. He, F. Y. Cui, D. Q. Gong, S. X. Hou, S. J. Xiong, X. J. Lei and Y. Q. Wei, *Eur. J. Pharm. Sci.*, 2009, **37**, 300–305.

164 K. Li, Y. Liu, K. Y. Pu, S. S. Feng, R. Zhan and B. Liu, *Adv. Funct. Mater.*, 2011, **21**, 287–294.

165 A. Singh, F. Dilnawaz, S. Mewar, U. Sharma, N. R. Jagannathan and S. K. Sahoo, *ACS Appl. Mater. Interfaces*, 2011, **3**, 842–856.

166 A. Aravind, S. H. Varghese, S. Veeranarayanan, A. Mathew, Y. Nagaoka, S. Iwai, T. Fukuda, T. Hasumura, Y. Yoshida, T. Maekawa and D. S. Kumar, *Cancer Nanotechnol.*, 2012, **3**, 1–12.

167 S. I. Thamake, S. L. Raut, Z. Gryczynski, A. P. Ranjan and J. K. Vishwanatha, *Biomaterials*, 2012, **33**, 7164–7173.

168 P. Liu, L. Qin, Q. Wang, Y. Sun, M. Zhu, M. Shen and Y. Duan, *Biomaterials*, 2012, **33**, 6739–6747.

169 P. Verderio, P. Bonetti, M. Colombo, L. Pandolfi and D. Prosperi, *Biomacromolecules*, 2013, **14**, 672–682.

170 J. M. Shen, F. Y. Gao, T. Yin, H. X. Zhang, M. Ma, Y. J. Yang and F. Yue, *Pharmacol. Res.*, 2013, **70**, 102–115.

171 M. F. Frasco, G. M. Almeida, F. Santos-Silva, M. Do Carmo Pereira and M. A. N. Coelho, *J. Biomed. Mater. Res., Part A*, 2015, **103**, 1476–1484.

172 H. Wang, Y. Zhao, H. Wang, J. Gong, H. He, M. C. Shin, V. C. Yang and Y. Huang, *J. Controlled Release*, 2014, **192**, 47–56.

173 R. Vivek, R. Thangam, V. Nipunbabu, C. Rejeeth, S. Sivasubramanian, P. Gunasekaran, K. Muthuchelian and S. Kannan, *ACS Appl. Mater. Interfaces*, 2014, **6**, 6469–6480.

174 Q. Liu, H. Zhu, J. Qin, H. Dong and J. Du, *Biomacromolecules*, 2014, **15**, 1586–1592.

175 F. Ye, Å. Barrefelt, H. Asem, M. Abedi-Valugerdi, I. El-Serafi, M. Saghafian, K. Abu-Salah, S. Alrokayan, M. Muhammed and M. Hassan, *Biomaterials*, 2014, **35**, 3885–3894.

176 R. Devulapally, N. M. Sekar, T. V. Sekar, K. Foygel, T. F. Massoud, J. K. Willmann and R. Paulmurugan, *ACS Nano*, 2015, **9**, 2290–2302.

177 M. Das, W. Duan and S. K. Sahoo, *Nanomedicine*, 2015, **11**, 379–389.

178 Y. Cui, M. Zhang, F. Zeng, H. Jin, Q. Xu and Y. Huang, *ACS Appl. Mater. Interfaces*, 2016, **8**, 32159–32169.

179 J. B. Du, Y. Cheng, Z. H. Teng, M. L. Huan, M. Liu, H. Cui, B. Le Zhang and S. Y. Zhou, *Mol. Pharm.*, 2016, **13**, 1711–1722.

180 J. Mosafer, K. Abnous, M. Tafaghodi, H. Jafarzadeh and M. Ramezani, *Colloids Surf., A*, 2017, **514**, 146–154.

181 M. Chatterjee, A. Hens, K. Mahato, N. Jaiswal, N. Mahato, Nagahanumaiah and N. Chanda, *J. Colloid Interface Sci.*, 2017, **506**, 126–134.

182 B. Sivakumar, R. G. Aswathy, R. Romero-Aburto, T. Mitcham, K. A. Mitchel, Y. Nagaoka, R. R. Bouchard, P. M. Ajayan, T. Maekawa and D. N. Sakthikumar, *Biomater. Sci.*, 2017, **5**, 432–443.

183 E. Kemal, T. F. Abelha, L. Urbano, R. Peters, D. M. Owen, P. Howes, M. Green and L. A. Dailey, *RSC Adv.*, 2017, **7**, 15255–15264.

184 Y. Malinovskaya, P. Melnikov, V. Baklaushev, A. Gabashvili, N. Osipova, S. Mantrov, Y. Ermolenko, O. Maksimenko, M. Gorshkova, V. Balabanyan, J. Kreuter and S. Gelperina, *Int. J. Pharm.*, 2017, **524**, 77–90.

185 X. Shen, T. Li, Z. Chen, Y. Geng, X. Xie, S. Li, H. Yang, C. Wu and Y. Liu, *Int. J. Nanomed.*, 2017, **12**, 4299–4322.

186 M. H. M. Leung and A. Q. Shen, *Langmuir*, 2018, **34**, 3961–3970.

187 G. Arya, M. Das and S. K. Sahoo, *Biomed. Pharmacother.*, 2018, **102**, 555–566.

188 M. J. Ramalho, E. Sevin, F. Gosselet, J. Lima, M. A. N. Coelho, J. A. Loureiro and M. C. Pereira, *Int. J. Pharm.*, 2018, **545**, 84–92.

189 J. Xi, W. Wang, L. Da, J. Zhang, L. Fan and L. Gao, *ACS Biomater. Sci. Eng.*, 2018, **4**, 1083–1091.

190 H. Tonbul, A. Sahin, E. Tavukcuoglu, G. Esendagli and Y. Capan, *J. Drug Delivery Sci. Technol.*, 2019, **54**, 101380.

191 M. A. Vakilinezhad, A. Amini, T. Dara and S. Alipour, *Colloids Surf., B*, 2019, **184**, 110515.

192 Y. Zhong, T. Su, Q. Shi, Y. Feng, Z. Tao, Q. Huang, L. Li, L. Hu, S. Li, H. Tan, S. Liu and H. Yang, *Int. J. Nanomed.*, 2019, **14**, 8543–8560.

193 R. S. Prabhuraj, K. Bomb, R. Srivastava and R. Bandyopadhyaya, *J. Polym. Res.*, 2020, **27**, 133.

194 P. Wu, Q. Zhou, H. Zhu, Y. Zhuang and J. Bao, *BMC Cancer*, 2020, **20**, 1–10.

195 A. I. Fraguas-Sánchez, A. I. Torres-Suárez, M. Cohen, F. Delie, D. Bastida-Ruiz, L. Yart, C. Martin-Sabroso and A. Fernández-Carballido, *Pharmaceutics*, 2020, **12**, 1–19.

196 X. Yu, L. Sun, L. Tan, M. Wang, X. Ren, J. Pi, M. Jiang and N. Li, *AAPS PharmSciTech*, 2020, **21**, 85.

197 N. Brandhonneur, Y. Boucaud, A. Verger, N. Dumait, Y. Molard, S. Cordier and G. Dollo, *Int. J. Pharm.*, 2021, **592**, 120079.

198 S. Malik, J. Lim, F. J. Slack, D. T. Braddock and R. Bahal, *J. Controlled Release*, 2020, **327**, 406–419.